doi.org/10.26434/chemrxiv.12012411.v1

Ni(I)-Alkyl Complexes Bearing Phenanthroline Ligands: Experimental Evidence for CO2 Insertion at Ni(I) Centers

Rosie Somerville, Carlota Odena, Marc Obst, Nilay Hazari, Kathrin Hopmann, Ruben Martin

Submitted date: 20/03/2020 • Posted date: 23/03/2020

Citation information: Somerville, Rosie; Odena, Carlota; Obst, Marc; Hazari, Nilay; Hopmann, Kathrin; Martin, Ruben (2020): Ni(I)-Alkyl Complexes Bearing Phenanthroline Ligands: Experimental Evidence for CO2 Insertion at Ni(I) Centers. ChemRxiv. Preprint. https://doi.org/10.26434/chemrxiv.12012411.v1

ABSTRACT: Although the catalytic carboxylation of unactivated alkyl electrophiles has reached remarkable levels of sophistication, the intermediacy of (phenanthroline)Ni(I)-alkyl species – complexes proposed in numerous Ni-catalyzed reductive cross-coupling reactions – has been subject to speculation. Herein, we report the synthesis of such elusive (phenanthroline)Ni(I) species and their reactivity with CO2, allowing us to address a long-standing challenge related to metal-catalyzed carboxylation reactions.

Ni(I)-Alkyl Complexes Bearing Phenanthroline Ligands: Experimental Evidence for CO_2 Insertion at Ni(I) Centers

Rosie J. Somerville,[†¶] Carlota Odena,[†¶‡] Marc F. Obst,[¥‡] Nilay Hazari,[£] Kathrin H. Hopmann[¥*] and Ruben Martin[†§*]

[†] Institute of Chemical Research of Catalonia (ICIQ), The Barcelona Institute of Science and Technology, Av. Països Catalans 16, 43007 Tarragona, Spain

[¶] Departament de Química Analítica i Química Orgànica, Universitat Rovira i Virgili, c/Marcel·lí Domingo, 1, 43007 Tarragona, Spain

[§] ICREA, Passeig Lluís Companys, 23, 08010 Barcelona, Spain

[¥] Hylleraas Center for Quantum Molecular Sciences, Department of Chemistry, UiT The Arctic University of Norway, N-9307 Tromsø, Norway

[£] Department of Chemistry, Yale University, P.O. Box 208107, New Haven, Connecticut 06520, United States

Supporting Information Placeholder

ABSTRACT: Although the catalytic carboxylation of *unactivated* alkyl electrophiles has reached remarkable levels of sophistication, the intermediacy of (phenanthroline)Ni(I)-alkyl species – complexes proposed in numerous Ni-catalyzed reductive cross-coupling reactions – has been subject to speculation. Herein, we report the synthesis of such elusive (phenanthroline)Ni(I) species and their reactivity with CO_2, allowing us to address a long-standing challenge related to metal-catalyzed carboxylation reactions.

Over the last decade, the development of Ni-catalyzed reductive carboxylation reactions involving organic (pseudo)halides and carbon dioxide (CO_2) has received extensive attention as a new methodology for the preparation of a broad range of synthetically useful carboxylic acids.[1] Among the wide variety of Ni-catalyzed reductive carboxylation reactions developed to date, the carboxylation of *unactivated* alkyl (pseudo)halides possessing β-hydrogens was found to be particularly challenging.[2] This is likely due to the propensity of the alkyl nickel intermediates that are formed via C(sp^3)–(pseudo)halide scission to undergo unproductive reduction, β-hydride elimination, and homocoupling reactions.[3] Although nickel catalysts supported by (di)phosphine or *N*-heterocyclic carbene ligands are routinely employed in a myriad of Ni-catalyzed C–C and C–heteroatom bond-forming reactions,[4] only finely-tuned derivatives of 1,10-phenanthroline (phen) ligands have enabled the carboxylation of *unactivated* alkyl electrophiles at either the initial C(sp^3)–X (X = Br, Cl, OSO_2R) site or at remote C(sp^3)–H bonds via chain-walking of the Ni catalyst along the alkyl side chain (Scheme 1).[2,5] Furthermore, a careful analysis of the literature indicates that phen-type ligands are also crucial for a number of Ni-catalyzed cross-couplings of *unactivated* alkyl halides, indicating that the importance of these ligands extends beyond carboxylation reactions.[4a,6]

Scheme 1. Carboxylation of Unactivated Alkyl Electrophiles.

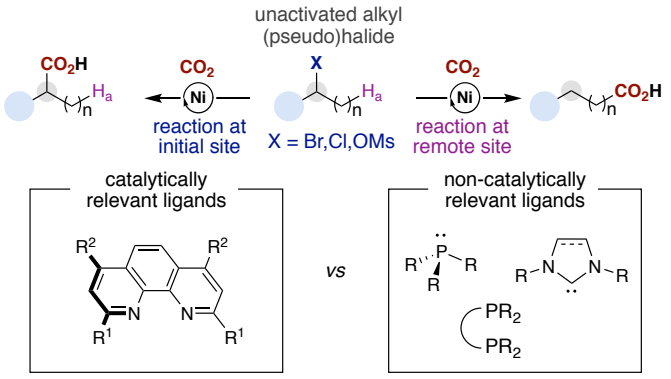

Despite the significant advances realized in methodology design, the mechanism of the Ni-catalyzed reductive carboxylation of *unactivated* alkyl (pseudo)halides with CO_2 is poorly understood. At present, our knowledge is primarily based on studies using *aryl* (pseudo)halides as substrates, which suggest a pathway involving CO_2 insertion into a (phen)Ni(I)–alkyl complex as a crucial elementary step (Scheme 2, *left*).[7,8] However, it is worth noting that none of these (phen)Ni(I)–alkyl intermediates have been structurally characterized or even observed spectroscopically, probably due to the fleeting nature and high reactivity of these paramagnetic Ni(I) species.[9] Elegant efforts towards this goal have recently been described by Diao, culminating in the characterization of well-defined (diphosphine)Ni(I)–alkyl complexes and investigations into their reactivity with CO_2.[10] Unfortunately, diphosphine ligands have not been shown to facilitate the Ni-catalyzed carboxylation of *unactivated* alkyl (pseudo)halides (Scheme 1).[2,11] Therefore, a systematic study aimed at preparing well-defined Ni(I)–alkyl complexes bearing catalytically-relevant phen ligands would represent: (a) an opportunity to study the reactivity of elusive Ni(I)–alkyl complexes supported by nitrogen-donor ligands, (b)

a foundation for investigating the mechanistic intricacies of catalytic reductive carboxylation reactions at the molecular level, and (c) a starting point for understanding issues related to the speciation of Ni catalysts supported by phen ligands in related cross-coupling and chain-walking reactions that employ *unactivated* alkyl halides or olefins, respectively.[4] Herein, we report the realization of these goals through the synthesis and isolation of Ni(I)–alkyl complexes bearing phen ligands, which enabled us to generate experimental evidence for rapid CO_2 insertion at Ni(I)–carbon bonds (Scheme 2, *right*). These results provide new vistas in catalytic carboxylation and cross-coupling reactions that may operate via Ni(I) complexes supported by phen ligands.[4,12]

Scheme 2. Proposed Reductive Carboxylation Mechanism via CO_2 Insertion at Phen-Ligated Ni(I)–Alkyl Species.

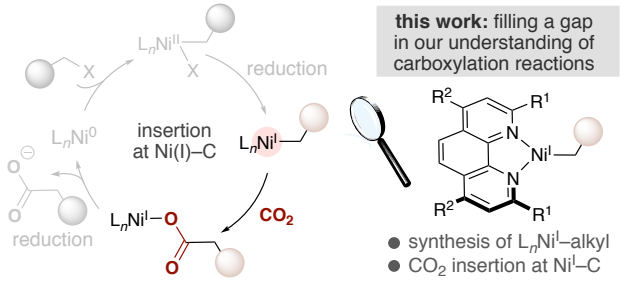

Our study began by establishing a robust and modular route to Ni(I)–halide species bearing phen ligands **L1** or **L2**. The choice of these ligands was not arbitrary, as placing bulky substituents adjacent to the nitrogen atom donor of the phen backbone is critical in Ni-catalyzed reductive carboxylation reactions of *unactivated* alkyl (pseudo)halides.[2] Steric shielding with the bulky mesityl substituents of **L1** may increase the likelihood of stabilizing our targeted Ni(I)–alkyl complexes, which are proposed to be highly reactive.[9] Additionally, **L2** was employed in the chain walking carboxylation of alkyl bromides.[2c] We envisioned that (**L**)Ni(I)–alkyl species could be accessed by alkylation of inner-sphere Ni(I)–halide complexes with an appropriate organometallic reagent. At the outset of our investigations, however, it was unclear whether an inner-sphere (**L**)Ni(I)–halide precursor could be obtained, as the closest related reported species with a phen-type ligand was the outer-sphere Ni(I) halide complex [Ni(**L**)$_2$]Cl, formed via oxidation of Ni(0)**L**$_2$ (**L** = 2,9-dimethyl-phen) with AgCl.[8,13,14] In order to avoid the synthesis of Ni(0)**L**$_2$ complexes and circumvent the purification steps required to remove oxidation byproducts, we hypothesized that inner sphere (**L**)Ni(I)X (X = Br, Cl) might be obtained via comproportionation of (**L**)NiX$_2$ with [Ni(COD)$_2$] in the presence of 1 equivalent of **L**.[13,14] This was indeed the case, and deep blue (**L**)Ni(I)X species were obtained in high yields (Scheme 2). The presence of the inner-sphere halide ligand was confirmed by X-ray crystallographic analysis of **1-Cl** and **2-Cl**. In addition, EPR spectroscopy of the four (**L**)Ni(I)X complexes at 77 K supports the presence of a Ni-centered radical. These results are noteworthy, as they represent examples of Ni(I) complexes bearing phen-type ligands with the halide directly coordinated to the Ni center.[14,15]

With a reliable route to (**L1,L2**)Ni(I)X in hand, we turned our attention to accessing the targeted Ni(I)–alkyl complexes via alkylation. An initial survey of Grignard reagents was carried out by monitoring the reactions using EPR spectroscopy to determine the stability of the resulting Ni(I)–alkyl complexes. As expected, the identity of the alkyl group, the reaction temperature, and the ligand employed all influenced the reaction outcome. For example, reactions with EtMgBr and MeMgCl resulted in negligible amounts of new metal-centered radicals, if any. Careful analysis of these reactions by NMR spectroscopy indicated the presence of Ni(0)**L**$_n$ complexes, suggesting decomposition pathways arising from β-hydride elimination, reduction, and/or homolytic cleavage.[16]

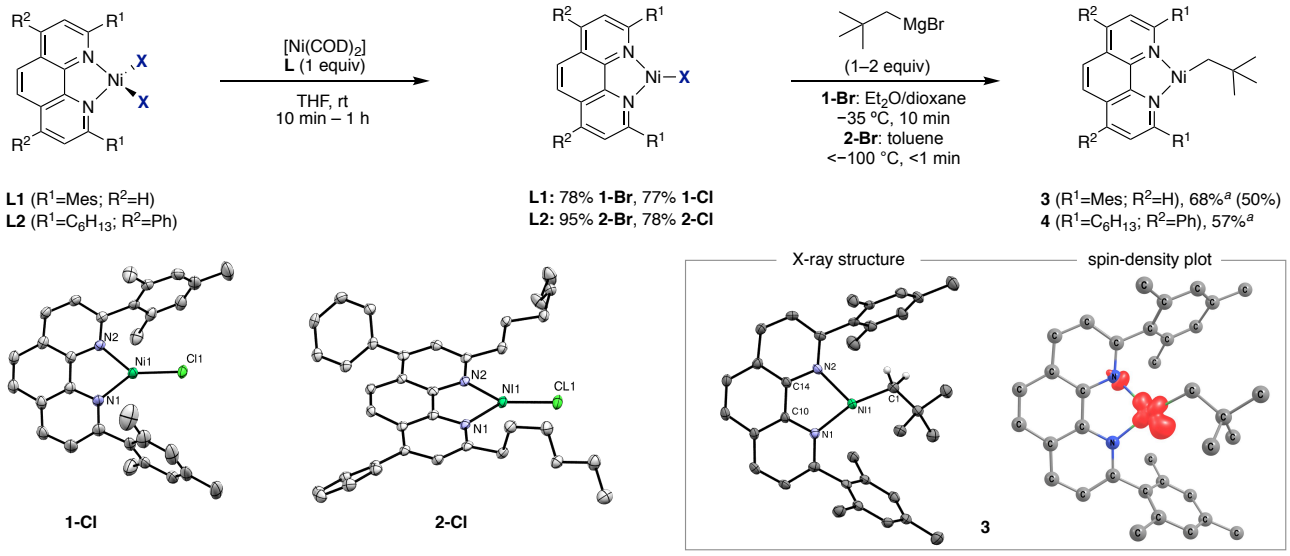

Figure 1. **Synthesis of Well-Defined Ni(I)–Alkyl Complexes Bearing phen Ligands**. X-ray crystallographic structures with thermal ellipsoids drawn at 50% probability levels. Selected distances (Å) and angles (°): **1-Cl**: Ni1–Cl1 2.1064(6). N1–Ni1–Cl1 140.24(6). N2–Ni1–Cl1 136.32(6). N2–Ni1–N1 83.44(8). **2-Cl**: Ni–Cl1 2.1417(9). N1–Ni–Cl1 133.80(8). N2–Ni–Cl1 142.61(9). (see SI for details). **3**: Ni–C1 1.961(3) Å, N1–Ni–C1 156.74(14), C1–Ni–N2 114.25(13), N1–Ni–N2 82.69(11). Bottom left: calculated spin-density plot of **3** with spin population of 0.94 on Ni (PBE-D3BJ/def2-TZVP, isovalue=0.01, see Figure S31).[a] Yield determined by EPR spectroscopy against Cu(II) standards. All other yields in Figure 1 are isolated yields (0.015 mmol scale for **3**). See SI for details.

Gratifyingly, however, the reactions of **1-Br** and **2-Br** with neopentylMgBr resulted in new rhombic EPR spectra, suggesting that the desired alkylation may have taken place.[17] Low-temperature crystallization (–35 ºC) furnished deep green crystals suitable for X-ray diffraction and allowed us to identify three-coordinate [(**L1**)Ni(I)CH_2tBu] (**3**) (Figure 1, right). DFT calculations support a Ni(I) description of **3**, with one unpaired electron centered on the Ni center (Figure 1 and Figure S31). The synthesis of **3** is particularly noteworthy; to the best of our knowledge, it represents the first Ni(I)–alkyl complex to be obtained with a catalytically relevant phen-type ligand. The Ni–C bond distance of 1.961(3) Å is similar to that of Ni(I) complexes bearing phosphine or NHC ligands.[10,18] The Ni coordination plane is offset by ca. 23° from the mean plane through **L1**, presumably due to the steric bulk of the neopentyl fragment. Interestingly, the N–Ni–C angles in **3** are 114.25(13)° and 156.74(14)°. The distortion of **3** to a T-shaped geometry is similar to that displayed for related diphosphine species [(dtbpe)Ni(CH_2tBu)] (110.97(8)° and 157.82(8)°, dtbpe = 1,2-bis(di-tert-butylphosphino)ethane).[18a] This geometry is electronically favored for a range of three-coordinate Ni(I) complexes and differs from the Y-shaped geometry of **1-Cl** and **2-Cl**.[19,20] At present, we propose that the geometry of the latter complexes is due to the π-donating nature of the chloride ligand, which has previously been shown to favor Y-shaped structures.[19] Alkylation of **2-Br** at low temperature gave [(**L2**)Ni(I)CH_2tBu] (**4**) in a 57% yield as estimated by EPR spectroscopy against a Cu(II) standard. Unfortunately, its instability prevented its isolation or characterization by X-ray diffraction.

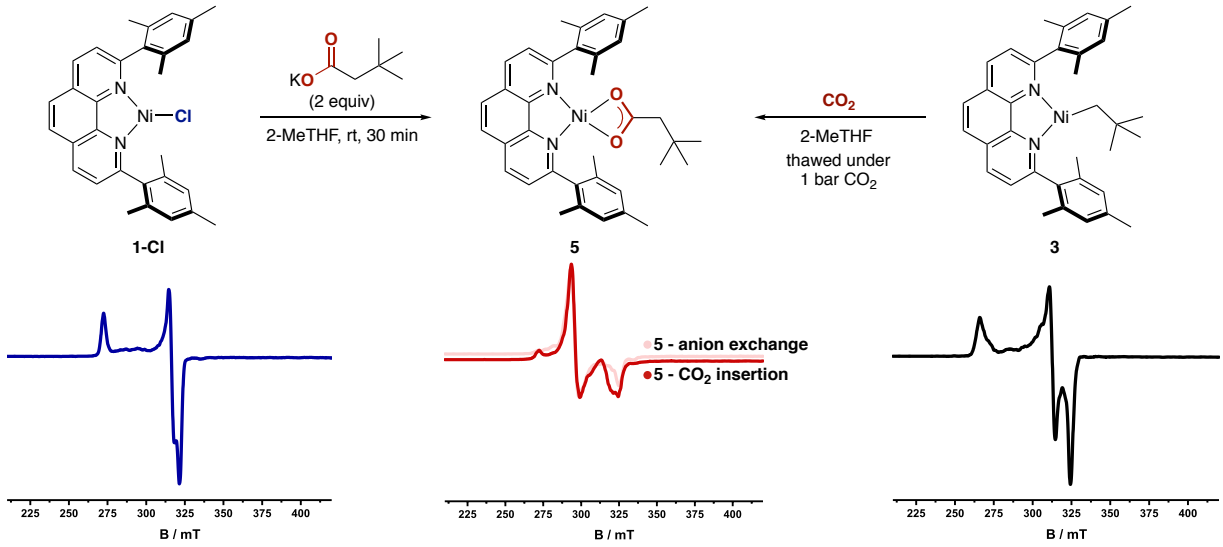

Figure 2. CO_2 Insertion at Ni(I) Centers. Top: Anion metathesis reaction (left) and CO_2 insertion into **3** (right) to synthesize **5**; Bottom: Change in 77 K EPR spectrum after anion metathesis (left) and after CO_2 insertion (right). Overlay of EPR spectra from both reactions shown in red.

Next, we turned our attention to investigating CO_2 insertion into the Ni(I)–C bond en route to Ni(I) carboxylate complexes, the key elementary step proposed in the catalytic carboxylation of alkyl (pseudo)halides (Figure 2).[7,8] Prior to these insertion experiments, however, anion metathesis reactions between **1-Cl** and tBuCH_2CO_2K were performed in order to obtain reference EPR and IR spectra of the proposed CO_2 insertion product (Figure 2, *left*). Gratifyingly, spectroscopic analysis of the reaction mixture showed the formation of a complex distinct from both **3** and **1-Cl** and supported the formation of Ni(I)–carboxylate complex **5**. Specifically, the band in the IR spectrum at 1543 cm^{-1} is suggestive of a ν_{asym} carboxylate stretch.[21] Furthermore, although repeated attempts to crystallize **5** did not provide crystals suitable for X-ray diffraction, the observed stretching frequency combined with the absence of signals between 1200-1400 cm^{-1} suggests a κ^2-coordination of the carboxylate fragment to the Ni(I) center.[21a] This was supported by DFT calculations that suggest a pseudotetrahedral geometry for **5** (Figure 3, *right*), with a computed carboxylate stretching frequency of 1484 cm^{-1} (SI, Figure S32). With these results in hand, we next investigated the reaction between **3** and CO_2 (1 bar) at –60 ºC (Figure 2, *right*). Analysis by EPR spectroscopy at 77 K showed the disappearance of the rhombic signal of **3** and the appearance of a new pseudoaxial signal with g_x, $g_y > g_z$ comparable to that of **5** (Figure 2, *centre*). Furthermore, comparison of the IR spectra of the product of direct CO_2 insertion into **3** with those of **5** showed an identical $\nu_{asym}CO_2$ stretch at 1543 cm^{-1}. Particularly illustrative was the absence of this signal and appearance of new signals at lower wavenumber upon performing the reaction with $^{13}CO_2$, which suggests that **5** is formed via CO_2 insertion at the Ni(I)–carbon center. Calculations predict a 34 cm^{-1} shift to lower wavenumbers upon incorporation of ^{13}C, consistent with the observed shift of 38 cm^{-1} to a band at 1505 cm^{-1} (Figure S18).[22] This was also corroborated indirectly by quenching in situ-generated **5** with dilute HCl and observing a 52% yield of *tert*-butylacetic acid (Scheme 3, *top*). Overall, these results are in agreement with DFT calculations that indicate facile CO_2 insertion into the Ni(I)–C bond of **3**, with a free energy barrier of

just 7.7 kcal mol^{-1} relative to **3** and free CO_2 (298.15 K). At the transition state (TS), CO_2 is bent (137°) and shows significant interactions with the Ni center (Figure 3, *left*). Although an outer-sphere insertion where CO_2 does not directly interact with the metal center might be conceivable, the computed transition state for this pathway showed a significantly higher barrier of 22.7 kcal mol^{-1} (Figure S35, Table S4).[23] Although these results are in line with the inner sphere pathway calculated for the Ni-catalyzed reductive carboxylation of benzyl halides with monodentate PCp_3 ligands,[24] our data contrast with the outer sphere pathway recently described for (Xantphos)Ni(I)-methyl[9] and pincer(PCP)-Ni(II)-methyl complexes, thus showing the subtleties exerted by the nature of the ligand backbone on CO_2 insertion.[25]

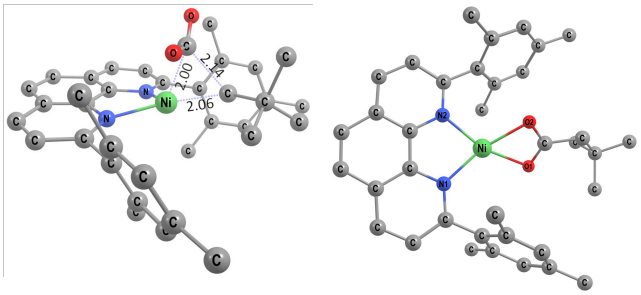

Figure 3. DFT Calculations. Optimized geometry of the preferred transition state for the insertion of CO_2 into **3** (left) and calculated geometry of **5** (right). (PBE-D3BJ/def2-TZVP/IEFPCM, hydrogen atoms omitted for clarity, distances in Å).

Given the relevance of **L2** in catalytic carboxylation reactions, attempts were made to enable CO_2 insertion at **4**. Although the sensitivity of **4** prevented the removal of $MgBr_2$ – the byproduct obtained by reacting (**L2**)Ni(I)Br with 1 equivalent of neopentylMgBr – a 50% yield of *tert*-butylacetic acid was obtained upon exposure of **4** to CO_2 (1 bar) at 77 K (Scheme 3, *bottom*). Interestingly, the reaction mixture rapidly turned blue upon CO_2 addition and only **2-Br** was observed when the reaction was analyzed by EPR spectroscopy. This suggested that the **L2** carboxylate complex [(**L2**)Ni(I)O_2CCH_2tBu] (**6**) resulting from CO_2 insertion underwent rapid halide exchange with $MgBr_2$ to form blue **2-Br**. Given the wide number of Ni-catalyzed reductive cross-coupling reactions that employ MgX_2 (X = Br, Cl) salt additives,[26] the formation of **2-Br** from in situ generated **4** provides evidence that halide complexes might be formed prior to reduction to the propagating Ni(0)$\mathbf{L}_n$ species within the catalytic cycle.[27]

Scheme 3. CO_2 Insertion en route to *t*BuCH$_2$CO$_2$H.

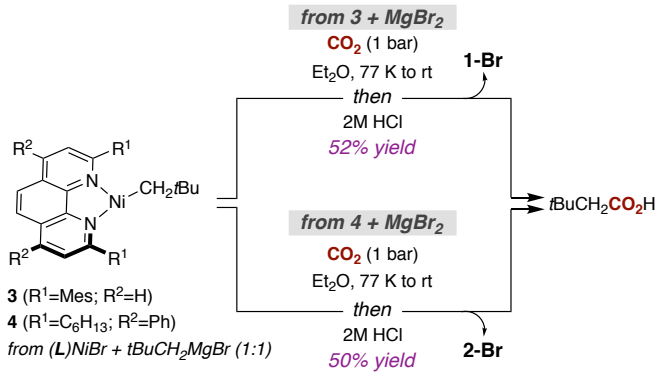

In conclusion, we have investigated the synthesis and CO_2 insertion of Ni(I)–alkyl complexes bearing catalytically relevant phen-type ligands. We have obtained experimental evidence for the rapid insertion of CO_2 into Ni(I)–C bonds, which is a long-presumed elementary step in the reductive carboxylation of alkyl (pseudo)halides. Given the important role exerted by phen ligands in many Ni-catalyzed cross-coupling reactions, these results might foster new investigations into the catalytic relevance of Ni(I)-alkyl complexes. Further investigations along these lines are currently underway in our laboratories.

AUTHOR INFORMATION

Corresponding Author

* rmartinromo@iciq.es; kathrin.hopmann@uit.no

Author contributions

‡ These authors contributed equally.

Funding Sources

No competing financial interests have been declared.

ACKNOWLEDGMENT

R.M., R.J.S., and C.O. thank ICIQ, FEDER/MICIU – AEI/ PGC2018- 096839-B-100, and funding from "la Caixa" Foundation (ID 100010434) under the agreement LCF/BQ/ SO15/52260010 for financial support. R.J.S. sincerely thanks "la Caixa" for a predoctoral fellowship. NH acknowledges support from the NIHGMS under Award Number R01GM120162. K.H.H and M.O. acknowledge the Research Council of Norway (Grant 262695), the Tromsø Research Foundation (Grant TFS2016KHH), NordForsk (Grant No. 85378) and Notur (Grants nn9330k, nn4654k). We also gratefully acknowledge the X-ray diffraction Research Support Area at ICIQ, Dr. Brandon Q. Mercado at Yale University for solving the structure of **1-Cl**, and Dr. Georgiana Stoica from the Spectroscopy and Material Characterization Unit at ICIQ for her help with EPR studies. We also thank Dr. Megan Mohadjer Beromi for insightful discussions.

REFERENCES

1. For selected reviews, see: (a) Burkart, M. D.; Hazari, N.; Tway, C. L.; Zeitler, E. L. Opportunities and Challenges for Catalysis in Carbon Dioxide Utilization. *ACS Catal.* **2019**, *9*, 7937. (b) Yang, Y.; Lee, J.-W. Toward Ideal Carbon Dioxide Functionalization. *Chem. Sci.* **2019**, *10*, 3905. (c) Tortajada, A.; Juliá-Hernández, F.; Börjesson, M.; Moragas, T.; Martin, R. Transition-Metal-Catalyzed Carboxylation Reactions with Carbon Dioxide. *Angew. Chem. Int. Ed.* **2018**, *57*, 15948. (d) Yeung, C. Photoredox Catalysis as a Strategy for CO_2 Incorporation: Direct Access to Carboxylic Acids from a Renewable Feedstock. *Angew. Chem. Int. Ed.* **2018**, *58*, 5492. (e) Artz, J.; Müller, T. E.; Thenert, K.; Kleinekorte, J.; Meys, R.; Sternberg, A.; Bardow, A.; Leitner, W. Sustainable Conversion of Carbon Dioxide: An Integrated Review of Catalysis and Life Cycle Assessment. *Chem. Rev.* **2018**, *118*, 434. (f) Cokoja, M.; Bruckmeier, C.; Rieger, B.; Herrmann, W. A.; Kühn, F. E. Transformation of Carbon Dioxide with Homogeneous Transition-Metal Catalysts: A Molecular Solution to a Global Challenge? *Angew. Chem. Int. Ed.* **2011**, *50*, 8510. (g) Huang, K.; Sun, C. L.; Shi, Z.-J. Transition-Metal-Catalyzed C–C Bond Formation through the Fixation of Carbon Dioxide. *Chem. Soc. Rev.*

2011, *40*, 2435. (h) *Carbon Dioxide as Chemical Feedstock*; Aresta, M., Ed.; Wiley VCH: Weinheim, **2010**. (i) Sakakura, T.; Choi, J. C.; Yasuda, H. Transformation of Carbon Dioxide. *Chem. Rev.* **2007**, *107*, 2365.

2. For selected references: (a) Sahoo, B.; Bellotti, P.; Juliá-Hernández, F.; Meng, Q. –Y.; Crespi, S; König, B.; Martin, R. Site-Selective Remote sp^3 C–H Carboxylation Enabled by the Merger of Photoredox and Nickel Catalysis. *Chem. Eur. –J.* **2019,** *25*, 9001. (b) Meng, Q. –Y.; Wang, S.; König, B. Carboxylation of Aromatic and Aliphatic Bromides and Triflates with CO_2 by Dual Visible-Light Nickel Catalysis. *Angew. Chem. Int. Ed.* **2017**, *56*, 13426. (c) Juliá-Hernández, F.; Moragas, T.; Cornella, J.; Martin, R. Remote Carboxylation of Halogenated Aliphatic Hydrocarbons with Carbon Dioxide. *Nature* **2017**, *545*, 84. (d) Börjesson, M.; Moragas, T.; Martin, R. Ni-Catalyzed Carboxylation of Unactivated Alkyl Chlorides with CO_2. *J. Am. Chem. Soc.* **2016**, *138*, 7504. (e) Wang, X.; Liu, Y.; Martin, R. Ni-Catalyzed Divergent Cyclization/Carboxylation of Unactivated Primary and Secondary Alkyl Halides with CO_2. *J. Am. Chem. Soc.* **2015**, *137*, 6476. (f) Liu, Y.; Cornella, J.; Martin, R. Ni-Catalyzed Carboxylation of Unactivated Primary Alkyl Bromides and Sulfonates with CO_2. *J. Am. Chem. Soc.* **2014**, *136*, 11212.
3. For selected reviews on the use of unactivated alkyl electrophiles in cross-coupling reactions, see: (a) Kambe, N.; Iwasaki, T.; Terao, J. Pd-Catalyzed Cross-Coupling Reactions of Alkyl Halides. *Chem. Soc. Rev.* **2011**, *40*, 4937. (b) Hu, X. Nickel-Catalyzed Cross-Coupling of Non-Activated Alkyl Halides: A Mechanistic Perspective. *Chem. Sci.* **2011**, *2*, 1867. (c) Jana, R.; Pathak, T. P.; Sigman, M. S. Advances in Transition Metal (Pd,Ni,Fe)-Catalyzed Cross-Coupling Reactions Using Alkyl-Organometallics as Reaction Partners. *Chem. Rev.* **2011**, *111*, 1417.
4. For excellent authoritative reviews on Ni catalysis, see: (a) Diccianni, J. B.; Diao, T. Mechanisms of Nickel-Catalyzed Cross-Coupling Reactions. *Trends Chem.* **2019**, *1*, 830. (b) Richmond, E.; Moran, J. Recent Advances in Nickel Catalysis Enabled by Stoichiometric Metallic Reducing Agents. *Synthesis* **2018**, *50*, 499. (c) Ananikov, V. P. Nickel: The "Spirited Horse" of Transition Metal Catalysis. *ACS Catal*. **2015**, *5*, 1964. (d) Tasker, S.; Standley, E.; Jamison, T. Recent Advances in Homogeneous Nickel Catalysis. *Nature* **2014**, *509*, 299.
5. For a recent review on Ni-catalyzed chain-walking reactions: Janssen-Müller, D.; Sahoo, B.; Sun, S.-Z.; Martin, R. Tackling Remote Sp^3 C−H Functionalization via Ni-Catalyzed "Chain-walking" Reactions. *Isr. J. Chem.* **2020**, DOI:10.1002/ijch.201900072.
6. Selected reviews on Ni-catalyzed cross-coupling reactions including those that make use of phen-type ligands: (a) Goldfogel, M.J., Huang, L. and Weix, D.J. (2019). Cross-Electrophile Coupling. In *Nickel Catalysis in Organic Synthesis*, S. Ogoshi (Ed.), Wiley Online Library, **2019**; pp 183–222. (b) Gu, J.; Wang, X.; Xue, W.; Gong, H. Nickel-Catalyzed Reductive Coupling of Alkyl Halides with Other Electrophiles: Concept and Mechanistic Considerations. *Org*. *Chem*. *Front*. **2015**, *2* (10), 1411. (c) Hu, X. Nickel-Catalyzed Cross Coupling of Non-Activated Alkyl Halides: A Mechanistic Perspective. *Chem*. *Sci*. **2011**, *2* (10), 1867.
7. Obst, M.; Pavlovic, L.; Hopmann, K. H. Carbon-Carbon Bonds with CO_2: Insights from Computational Studies. *J. Organomet. Chem.* **2018**, *864*, 115.
8. Somerville, R. J.; Martin, R. Relevance of Ni(I) in Catalytic Carboxylation Reactions. In *Nickel Catalysis in Organic Synthesis*; Ogoshi, S., Ed.; Wiley Online Library, 2019; pp 285–330.
9. For a recent example of Ni(I)-*aryl* complexes bearing *N*-donor ligands: Mohadjer Beromi, M.; Brudvig, G. W.; Hazari, N.; Lant, H. M. C.; Mercado, B. Q. Synthesis and Reactivity of Paramagnetic Polypyridyl Ni Complexes Relevant to $C(Sp^2)$–$C(Sp^3)$ Coupling Reactions. *Angew. Chem. Int. Ed.* **2019**, *58*, 6094.
10. Diccianni, J. B.; Hu, C. T.; Diao, T. Insertion of CO_2 Mediated by a (Xantphos)Ni^{I}–Alkyl Species. *Angew. Chem. Int. Ed.* **2019**, *58*, 13865.
11. For control experiments using ^{tBu}Xantphos in the catalytic carboxylation of unactivated alkyl halides, see the Supporting Information.
12. For reviews on Ni-catalyzed reductive cross-coupling reactions: Gu, J.; Wang, X.; Xue, W.; Gong, H. Nickel-Catalyzed Reductive Coupling of Alkyl Halides with other Electrophiles: Concept and Mechanistic Considerations. *Org. Chem. Front.* **2015**, *3*, 1411. (b) Weix, J. D. Methods and Mechanisms for Cross-Electrophile Coupling of Csp^2 Halides with Alkyl Electrophiles. *Acc. Chem. Res.* **2015**, *48*, 1767. (c) Moragas, T.; Correa, A.; Martin, R. Metal-Catalyzed Reductive Coupling Reactions of Organic Halides with Carbonyl-Type Compounds. *Chem. Eur. J.* **2014**, *20*, 8242. (d) Knappke, C. E. I.; Grupe, S.; Gärtner, D.; Corpet, M.; Gosmini, C.; Jacobi von Wangelin, A. Reductive Cross-Coupling Reactions between Two Electrophiles *Chem. Eur. J.* **2014**, *20*, 6828.
13. During the course of our studies, a comproportionation route to inner-sphere Ni(I)-halide complexes was reported: Zarate, C.; Yang, H.; Bezdek, M. J.; Hesk, D.; Chirik, P. J. Ni(I)–X Complexes Bearing a Bulky α-Diimine Ligand: Synthesis, Structure, and Superior Catalytic Performance in the Hydrogen Isotope Exchange in Pharmaceuticals. *J. Am. Chem. Soc.* **2019**, *141*, 5034.
14. During the course of our studies, an inner-sphere bromide complex bearing a bulky bipyridine ligand was reported via reduction of a Ni(II) complex: Lin, Q.; Diao, T. Mechanism of Ni-Catalyzed Reductive 1,2-Dicarbofunctionalization of Alkenes. *J. Am. Chem. Soc.* **2019**, *141*, 17937.
15. **2-Br** and **L1** were competent as precatalyst and ligand, respectively, for the chain-walking carboxylation of 2-bromoheptane. See Supporting Information and ref. 2c for details.
16. It is worth noting that Ni(**L2**)$_2$ was detected when **L2** complexes were employed (see ref. 2c). For reactions with **L1**-bearing complexes, unusual [Ni(**L1**)]$_3$ and [Ni(**L4**)]$_4$ trimers and tetramers crystallised from the reaction mixtures (see the Supporting Information for details).
17. Reactions between **1-Cl** or **2-Cl** and neopentylMgBr also form **3**.
18. (a) Kitiachvili, K. D.; Mindiola, D. J.; Hillhouse, G. L. Preparation of Stable Alkyl Complexes of Ni(I) and Their One-Electron Oxidation to Ni(II) Complex Cations. *J. Am. Chem. Soc.* **2004**, *126*, 10554. (b) Laskowski, C. A.; Bungum, D. J.; Baldwin, S. M.; Del Ciello, S. A.; Iluc, V. M.; Hillhouse, G. L. Synthesis and Reactivity of Two-Coordinate Ni(I) Alkyl and Aryl Complexes. *J. Am. Chem. Soc.* **2013**, *135*, 18272.
19. For a selection of T-shaped Ni(I) complexes, see: (a)

Kogut, E.; Wiencko, H. L.; Zhang, L.; Cordeau, D. E.; Warren, T. H. A Terminal Ni(III)-Imide with Diverse Reactivity Pathways. *J. Am. Chem. Soc.* **2005**, *127*, 11248. (b) Eckert, N. A.; Dinescu, A.; Cundari, T. R.; Holland, P. L. A T-Shaped Three-Coordinate Nickel(I) Carbonyl Complex and the Geometric Preferences of Three-Coordinate d^9 Complexes. *Inorg. Chem.* **2005**, *44*, 7702. (c) Iluc, V. M.; Hillhouse, G. L. Three-Coordinate Nickel Carbene Complexes and Their One-Electron Oxidation Products. *J. Am. Chem. Soc.* **2014**, *136*, 6479.

20. For information about the geometries of three-coordinate d^9 complexes, see: (a) Alvarez, S. Bonding and Stereochemistry of Three-Coordinated Transition Metal Compounds. *Coord. Chem. Rev.* **1999**, *193–195*, 13. (b) Jean, Y.; Marsden, C. T. *Molecular Orbitals of Transition Metal Complexes*; OUP Oxford, 2005.
21. (a) Deacon, G. B.; Phillips, R. J. Relationships between the Carbon-Oxygen Stretching Frequencies of Carboxylato Complexes and the Type of Carboxylate Coordination. *Coord. Chem. Rev.* **1980**, *33*, 227. (b) Nara, M.; Torii, H.; Tasumi, M. Correlation between the Vibrational Frequencies of the Carboxylate Group and the Types of Its Coordination to a Metal Ion: An Ab Initio Molecular Orbital Study. *J. Phys. Chem.* **1996**, *100*, 19812.
22. A calculated shift of 34 cm^{-1} from 1484 cm^{-1} to 1450 cm^{-1} (PBE).
23. Hazari, N.; Heimann, J. E. Carbon Dioxide Insertion into Group 9 and 10 Metal-Element σ Bonds. *Inorg. Chem.* **2017**, *56* (22), 13655–13678.
24. Sayyed, F. B.; Sakaki, S. The crucial roles of $MgCl_2$ as a non-innocent additive in the Ni-catalyzed carboxylation of benzyl halide with CO_2 *Chem. Commun.* **2014**, *50*, 13026.
25. (a) Schmeier, T. J.; Hazari, N.; Incarvito, C. D.; Raskatov, J. A. Exploring the Reactions of CO_2 with PCP Supported Nickel Complexes. *Chem. Commun.* **2011**, *47*, 1824. (b) Jonasson, K. J.; Wendt, O. F. Synthesis and Characterization of a Family of POCOP Pincer Complexes with Nickel: Reactivity towards CO_2 and Phenylacetylene. *Chem. Eur. J.* **2014**, *20*, 11894.
26. Selected examples where MgX_2 additives are employed in Ni-catalyzed reductive cross-coupling reactions: (a) Ye, Y.; Chen, H.; Yao, K.; Gong, H. Iron-Catalyzed Reductive Vinylation of Tertiary alkyl Oxalates with Activated Vinyl Halides. *Org. Lett.* **2020**, *22*, 2070 (b) Gao, M.; Sun, D.; Gong, H. Ni-Catalyzed Reductive C–O Bond Arylation of Oxalates Derived from α-Hydroxy Esters with Aryl Halides. *Org. Lett.* **2019**, *21*, 1645. (c) Wang, X.; Ma, G.; Peng, Y.; Pitsch, C. E.; Moll, B. J.; Ly, T. D.; Wang, X.; Gong, H. Ni-Catalyzed Reductive Coupling of Electron-Rich Aryl Iodides with Tertiary Alkyl Halides. *J. Am. Chem. Soc.* **2018**, *140*, 14490. (d) Fujihara, T.; Horimoto, Y.; Mizoe, T.; Sayyed, F. B.; Tani, Y.; Terao, J.; Sakaki, S.; Tsuji, Y. Nickel-Catalyzed Double Carboxylation of Alkynes Employing Carbon Dioxide. *Org. Lett.* **2014**, *16*, 4960. (e) Leon, T.; Correa, A.; Martin, R. Nickel-Catalyzed Direct Carboxylation of Benzyl Halides *J. Am. Chem. Soc.* **2013**, *135*, 1221.
27. Charboneau, D. J.; Brudvig, G. W.; Hazari, N.; Lant, H. M. C.; Saydjari, A. K. Development of an Improved System for the Carboxylation of Aryl Halides through Mechanistic Studies. *ACS Catal.* **2019**, *9*, 3228.

Supporting Information

Ni(I)-Alkyl Complexes Bearing Phenanthroline Ligands: Experimental Evidence for CO_2 Insertion at Ni(I) Centers

Rosie J. Somerville,[†¶] Carlota Odena,[†¶‡] Marc F. Obst,[¥‡] Nilay Hazari,[£*] Kathrin H. Hopmann[¥*] and Ruben Martin[†§*]

[†] Institute of Chemical Research of Catalonia (ICIQ), The Barcelona Institute of Science and Technology, Av. Països Catalans 16, 43007 Tarragona, Spain

[¶] Departament de Química Analítica i Química Orgànica, Universitat Rovira i Virgili, c/Marcel·lí Domingo, 1, 43007 Tarragona, Spain

[§] ICREA, Passeig Lluís Companys, 23, 08010 Barcelona, Spain

[¥] Hylleraas Center for Quantum Molecular Sciences, Department of Chemistry, UiT The Arctic University of Norway, N-9307 Tromsø, Norway

[£] Department of Chemistry, Yale University, P.O. Box 208107, New Haven, Connecticut 06520, United States

Corresponding authors

Ruben Martin: rmartinromo@iciq.es

Kathrin Hopmann: kathrin.hopmann@uit.no

Table of Contents

[‡]These authors contributed equally.

General considerations

Reagents. $Ni(COD)_2$ and NiI_2 (99.99% trace metal basis) were purchased from Strem Chemicals. Neocuproine, bathocuproine, Mn powder (99.99% trace metal basis), 1-bromoheptane, and 2-bromoheptane were purchased from Sigma Aldrich. 2,9-Dichlorophenanthroline was purchased from Fluorochem. Anhydrous *N,N*-dimethylformamide (DMF) was purchased from Acros Organics. **L3** (*t*Bu-Xantphos) was purchased from DSC.
Neopentylmagnesium bromide was synthesized following a reported procedure.[1]
L1[2] and **L2**[3,4] were synthesised according to literature procedures. Potassium carboxylate salt $tBuCH_2CO_2K$ was synthesised by combining 2,3-dimethyl butyric acid with KOH in methanol followed by removal of the volatiles. All other reagents were purchased from commercial sources and used without further purification.

Solvents. Hydrocarbon solvents, 2-MeTHF, toluene-d_8, THF-d_8 and benzene-d_6 were degassed by the appropriate method (sparging or three freeze-pump-thaw cycles) then dried over 4Å molecular sieves and stored in the glovebox. Inhibitor-free THF and Et_2O were purified with an Innovative Technologies solvent purification system. $CDCl_3$ was used as received for NMR of air-stable Ni(II) complexes.

Analytical methods. Flash chromatography was performed with Sigma Aldrich technical grade silica gel 60 (230-400 mesh). Thin layer chromatography was carried out using Merck TLC Silica gel 60 F254. NMR spectra were recorded on Bruker Avance Ultrashield 300, 400, or 500 MHz spectrometers, with chemical shifts reported in parts per million (ppm) and coupling constants, *J*, reported in hertz. IR spectra were obtained with a Bruker FT-IR Alpha spectrometer inside the glovebox.

Continuous wave (CW) X-band EPR spectra were obtained using a Bruker EMX Micro X-band spectrometer using a Bruker ER 1164 HS resonator. Spectra were simulated using SpinFit within Xenon. The samples were cooled to 77 K in a Suprasil finger dewar (Wilmad-LabGlass) filled with liquid nitrogen. The spectral data were collected with the following spectrometer settings: microwave power = 0.56 mW; centre field = 3250 G, sweep width = 2500 G, sweep time = 35.07 s, modulation frequency = 100 KHz, modulation amplitude = 10 G, power attenuation = 25 dB, time constant = 20.48 ms. Sweep width of 3500 G and power of 0.346 mW were employed for obtaining the yield for the in situ syntheses of **3** and **4**. Simulations, g values, and frequencies are provided alongside the characterisation data of the complexes.
Evans method[5,6] solution magnetic susceptibility measurements were performed for [$NiBr_2$(**L2**)], **1-Cl**, **1-Br**, and **3**.

Dr Brandon Q. Mercado (Yale University) collected the X-ray data for **1-Cl** and refined and solved the structure (see X-ray crystallography section).

Preparation of nickel complexes

Nickel(II) dihalide precursors

[$NiCl_2$(L1)]

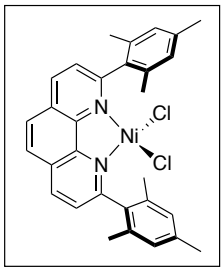

In a 12 mL vial, **L1** (175.4 mg, 0.421 mmol, 1 equiv) and $NiCl_2$·DME (92.5 mg, 0.421 mmol, 1 equiv) were combined in 4 mL THF. Stirring at room temperature for 45 minutes followed by sonication for 10 minutes gave a purple suspension. This was combined with 4 mL Et_2O then filtered, washed with further Et_2O (2 x 5 mL), and dried under vacuum to give paramagnetic [$NiCl_2$(**L1**)] as a pink solid (197 mg, 86% yield).

^{1}H NMR (500 MHz, $CDCl_3$): δ 73.78 (s, 2H, **L1**), 25.28 (s, 2H, **L1**), 24.71 (s, 2H, **L1**) 9.63 (s, 4H, **L1**-mes), 5.30 (s, 12 H, *ortho*-CH_3), 4.97 (br, $\Delta\nu_{1/2}$ = 41 Hz, 6 H, *para*-CH_3).
EA Calcd. C, 65.98; H, 5.17; N, 5.13; Found: C, 65.26; H, 5.40; N, 4.88.

[$NiBr_2$(L1)]

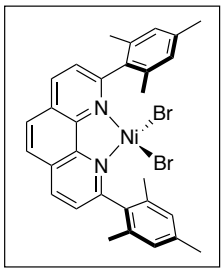

In a 12 mL vial, **L1** (80 mg, 0.192 mmol, 1 equiv) and $NiBr_2$·DME (59 mg, 0.192 mmol, 1 equiv) were combined in 2 mL THF. Sonication for 10 minutes gave a purple suspension that was filtered, washed with Et_2O, and dried under vacuum to give paramagnetic [$NiBr_2$(**L1**)] as a dark pink solid (101 mg, 83%).

^{1}H NMR (500 MHz, $CDCl_3$ (paramagnetic)): δ 73.78 (s, $\Delta\nu_{1/2}$ = 60 Hz, 2H, **L1**), 25.28 (s, 2H, **L1**), 24.71 (s, 2H, **L1**), 9.63 (s, 4H, **L1**-mes), 4.94 (s, 12 H, *ortho*-CH_3), 4.33 (br, $\Delta\nu_{1/2}$ = 70 Hz, 6 H, *para*-CH_3).
EA Calcd. C, 56.74; H, 4.44; N, 4.41; Found: C, 52.31; H, 4.41; N, 4.05. ($CHCl_3$ contaminant likely)

[$NiCl_2$(L2)]

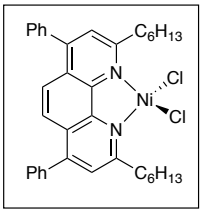

In a 12 mL vial, **L2** (200.6 mg, 0.401 mmol, 1 equiv) and $NiCl_2$·DME (88.0 mg, 0.401 mmol, 1 equiv) were combined in 3 mL THF. Stirring at room temperature for 45 minutes followed by sonication for 10 minutes gave a purple suspension. This was combined with 10 mL pentane then filtered, washed with further Et_2O (3 x 5 mL), and dried under vacuum to give paramagnetic [$NiCl_2$(**L2**)] as a pink solid (234.8 mg, 93% yield).

^{1}H NMR (400 MHz, $CDCl_3$): δ 82.40 (s, 2H, **L2**), 30.26 (br, $\Delta\nu_{1/2}$ = 450 Hz, 4H, CH_2), 28.40 (s, 2H, **L2**), 17.89 (s, 4H) , 9.43 (m, 4H, **L2**-Ph), 8.75 (m, 2H, **L2**-Ph), 7.23 (m, 4H, **L2**-Ph), 7.08 (s, 4H, CH_2), 3.95(s, 4H, CH_2), 2.73 (s, 4H, CH_2), 1.58 (m, 6H, CH_3).
EA Calcd. C, 68.60; H, 6.40; N, 4.44; found: C, 68.09; H, 6.27; N, 4.50.

[$NiBr_2$(L2)]

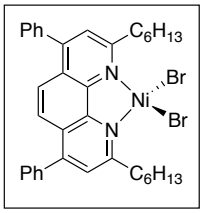

Synthesised following a modified literature procedure.[7]

To a mixture of $NiBr_2·3H_2O$ (99.0 mg, 0.363 mmol, 1 equiv) and **L2** (181.8 mg, 0.363 mmol, 1 equiv) was added 10 mL ethanol. The mixture was stirred under air at 40 °C for 30 minutes, then the purple solid was filtered off and washed with 2 x 10 mL anhydrous ethanol followed by 2 x 10 mL Et_2O. Drying under vacuum gave paramagnetic [$NiBr_2$(**L2**)] as a pink solid (166.4 mg, 64% yield).

^{1}H NMR (400 MHz, $CDCl_3$): δ 80.46 (br, $\Delta\nu_{1/2}$ = 80 Hz, 2H, **L2**), 29.06 (s, 2H, **L2**), 18.25 (br, $\Delta\nu_{1/2}$ = 800 Hz, 4H, CH_2), 13.88 (br, $\Delta\nu_{1/2}$ = 110 Hz, 4H, CH_2), 9.20 (m, 4H, **L2**-Ph), 8.61 (m, 2H, **L2**-Ph), 7.07 (m, 4H, **L2**-Ph), 4.66 (s, 4H, CH_2), 2.74 (s, 4H, CH_2), 2.06 (s, 4H, CH_2), 1.24 (s, 6H, CH_3).
Magnetic susceptibility (Evans method) μ_{eff} = 2.88 μ_B
EA Calcd. C, 60.12; H, 5.61; N, 3.89; Found C: 59.95; H: 5.47; N: 3.99

Nickel(I) halide complexes

The four Ni(I)-halide complexes below were synthesised by comproportionation (Scheme S1)

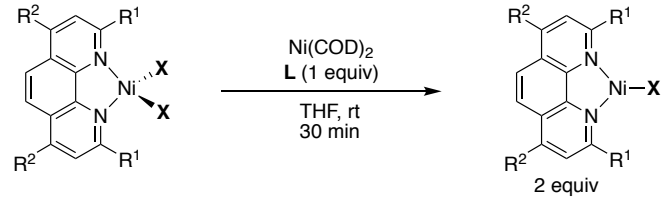

L1 (R^1=Mes; R^2=H)
L2 (R^1=C_6H_{13}; R^2=Ph)

L1: 78% **1-Br**, 77% **1-Cl**
L2: 95% **2-Br**, 78% **2-Cl**

Scheme S1. General method for synthesis of nickel(I) halide complexes.

[(L1)NiCl] (1-Cl)

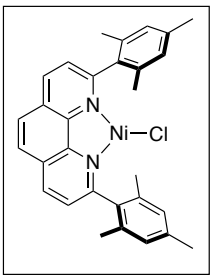

L1 (42.5 mg, 0.102 mmol, 1 equiv), [$NiCl_2$(**L1**)] (55.7 mg, 0.102 mmol, 1 equiv), and $Ni(COD)_2$ (28.1 mg, 0.102 mmol, 1 equiv) were combined in 2 mL THF. After stirring for 10 min at room temperature, the solution was filtered through glass fibre filter paper. This was washed with an additional 2.5 mL THF. The volatiles were then removed, the solid washed with pentane, then dried under vacuum to give **1-Cl** as a dark blue powder (80 mg, 77%).

^{1}H NMR (500 MHz, toluene-d_8): δ 33.38 (br, $\Delta\nu_{1/2}$ = 1200 Hz (approx.), 2H, **L1**), 10.75 (br, $\Delta\nu_{1/2}$ = 300 Hz (approx.), 2H, **L1**), 6.14 (br, $\Delta\nu_{1/2}$ = 850 Hz), 5.03 (br, $\Delta\nu_{1/2}$ = 400 Hz (approx.)), 2.11 (s).
The ^{1}H NMR spectrum is very broad and the signals were not able to be assigned to particular proton environments.
Magnetic susceptibility (Evans method) $\mu_{\mathbf{eff}}$ = 1.94 μ_B
EPR spectrum simulated with g_x = 2.084, g_y = 2.119, g_z = 2.461. lineshape = 0.8. The continuous wave EPR spectrum was obtained in 2-MeTHF at 9.386 GHz.

Single crystals of **1-Cl** were grown from toluene/pentane at −35 ºC.

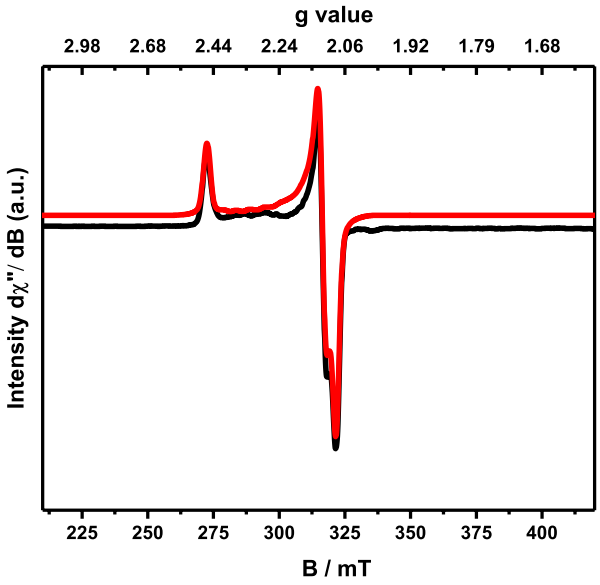

Figure S1. EPR spectrum of 1-Cl (77 K, 2-MeTHF). red = simulated spectrum.

[(L1)NiBr] (1-Br)

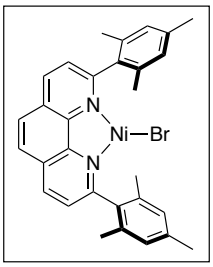

L1 (52.7 mg, 0.127 mmol, 1 equiv), [$NiBr_2$(**L1**)] (80.4 mg, 0.127 mmol, 1 equiv), and $Ni(COD)_2$ (28.1 mg, 0.127 mmol, 1 equiv) were combined in 4 mL THF. After stirring for 15 min at room temperature, the solution was filtered through glass fibre filter paper. This was washed with an additional 1 mL THF. The volatiles were then removed, the solid washed with pentane, then dried under vacuum to give **1-Br** as a dark blue powder (109.7 mg, 78%).

^{1}H NMR (500 MHz, toluene-d_8): δ 33.38 (br, $\Delta\nu_{1/2}$ = 1400 Hz (approx.), **L1**), 10.75 (br, $\Delta\nu_{1/2}$ = 255 Hz, **L1**), 6.14 (br s), 5.03 (br, $\Delta\nu_{1/2}$ = 360 Hz), 2.28 (br s).
The ^{1}H NMR spectrum is very broad and the signals were not able to be assigned to particular proton environments.
Magnetic susceptibility (Evans method) μ_{eff} = 1.87 μ_B
EPR spectrum simulated with g_x = 2.093, g_y = 2.129, g_z = 2.469. lineshape = 1. The continuous wave EPR spectrum was obtained at 9.389 GHz.

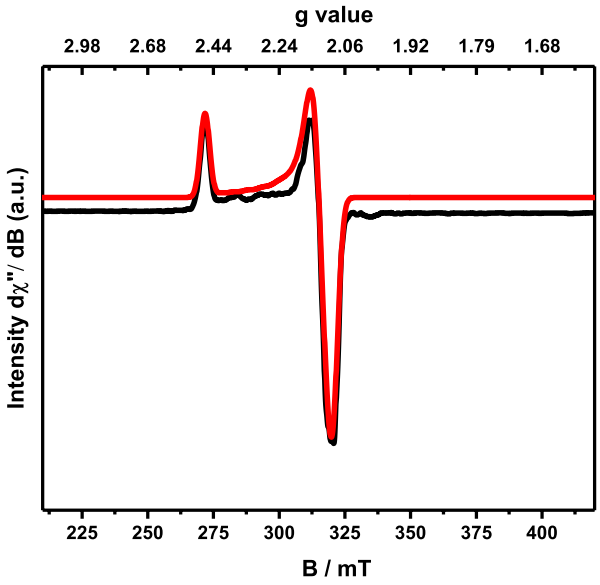

Figure S2. EPR spectrum of 1-Br (77 K, 2-MeTHF). red = simulated spectrum.

[(L2)NiCl] (2-Cl)

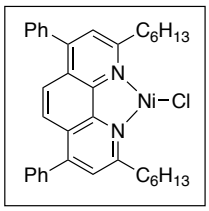

L2 (35.4 mg, 0.0707 mmol, 1 equiv), [$NiCl_2$(**L2**)] (44.6 mg, 0. 0707 mmol, 1 equiv), and $Ni(COD)_2$ (19.5 mg, 0. 0707 mmol, 1 equiv) were combined in 1 mL THF. After stirring for 1 h at room temperature, the solution was filtered through glass fibre filter paper. This was washed with an additional 1 mL THF. Pentane (2 mL) was then added and the solution placed in the freezer (−35 °C) overnight. The solid was filtered off, washed with cold pentane (2 mL), then dried under vacuum to give **2-Cl** as a deep blue crystalline solid (66.2 mg, 78%).

Crystals suitable for X-ray diffraction were obtained from this THF/pentane mixture at −35 ºC.

^{1}H NMR (400 MHz, toluene-d_8): δ 37.07 (br, $\Delta\nu_{1/2}$ = 1500 Hz (approx.), 2H, **L2**), 12.61 (br, $\Delta\nu_{1/2}$ = 300 Hz, 2H), 8.74 (s, **L2**-Ph), 8.62 (s, **L2**-Ph) [δ(8.74+8.62) = 10H], 5.72 (s, 6H, hexyl signals), 1.29 (br m, 20 H, hexyl signals). **EPR** spectrum simulated with g_x = 2.089, g_y = 2.114, g_z = 2.449. lineshape = 0.9. The continuous wave EPR spectrum was obtained at 9.384 GHz.

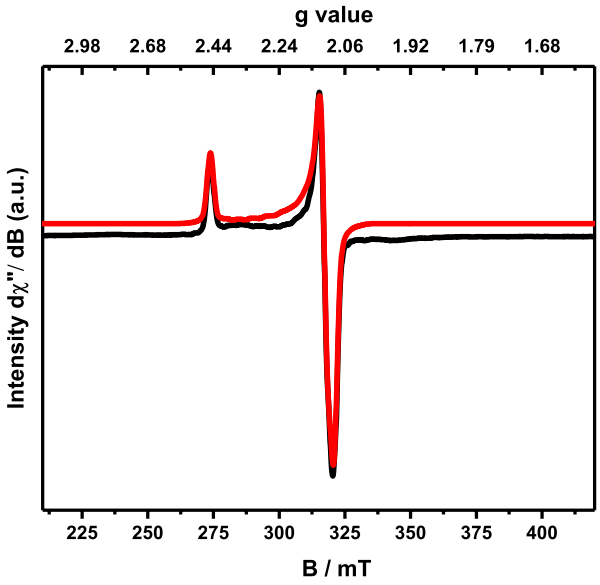

Figure S3. EPR spectrum of 2-Cl (77 K, 2-MeTHF). red = simulated spectrum.

[(L2)NiBr] (2-Br)

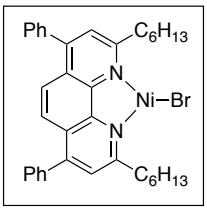

L2 (91.8 mg, 0.183 mmol, 1 equiv), [$NiBr_2$(**L2**)] (131.9 mg, 0.183 mmol, 1 equiv), and $Ni(COD)_2$ (50.44 mg, 0.183 mmol, 1 equiv) were combined in 3 mL THF. After stirring for 40 min at room temperature, the solution was filtered through glass fibre filter paper. This was washed with an additional 2 mL THF. The volatiles were then removed, the solid washed with pentane, then dried under vacuum to give **2-Br** as a dark blue powder (224 mg, 95%).

^{1}H NMR (400 MHz, toluene-d_8): δ 35.81 (very broad s, $\Delta\nu_{1/2}$ = 1500 Hz (approx.)), 12.40 (br, $\Delta\nu_{1/2}$ = 215 Hz, 2H, **L2**), 8.64 (s, **L2**-Ph), 8.50 (s, $\Delta\nu_{1/2}$ = 1500 Hz, **L2**-Ph) [δ(8.74+8.62) = 8H], 5.79 (s, 5H), 1.25 (m). Some signals are extremely broad.

EPR spectrum simulated with $g_x = 2.090$, $g_y = 2.126$, $g_z = 2.458$. lineshape = 1. The continuous wave EPR spectrum was obtained at 9.390 GHz.

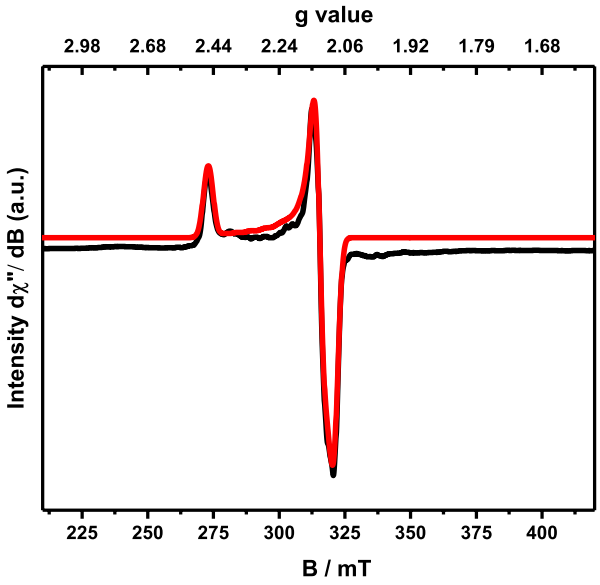

Figure S4. EPR spectrum of 2-Br (77 K, 2-MeTHF). red = simulated spectrum.

Nickel(I) alkyl complexes

[(L1)Ni(CH$_2$*t*Bu)] (3)

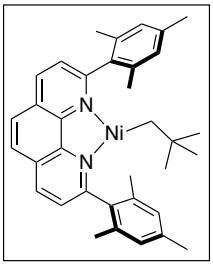

A suspension of **1-Br** (7.8 mg, 0.014 mmol, 1 equiv) in 1.5 mL Et_2O was cooled to −35 ºC. A solution of neopentylMgBr (140 µL, 0.2 M in THF, 2 equiv) was then added. The vial was agitated until the dark blue **1-Br** had disappeared (ca. 5 min). The deep green reaction mixture was filtered through glass fibre filter paper to remove unreacted **1-Br** and some $MgBr_2$, then dioxane (200 µL) was added to precipitate the magnesium salts. The cloudy solution was placed in the glovebox freezer for 10 minutes (−35 ºC) then filtered through 1.5 cm of celite in a pipette. Volatiles were removed then the dark green residue was extracted with 3 mL pentane. The pentane extracts were filtered through celite, then pentane was removed to give **3** as a dark green solid (3.9 mg, 50%).

Single crystals were obtained from an Et_2O/pentane mixture at −35 ºC.

^{1}H NMR (500 MHz, toluene-d_8): δ 55.35 (br, $\Delta\nu_{1/2}$ = 1500 Hz (approx.), **L1**), 43.97 (br, $\Delta\nu_{1/2}$ = 1700 Hz (approx.), **L1**), 13.68 (br, $\Delta\nu_{1/2}$ = 185 Hz), 10.74 (br, $\Delta\nu_{1/2}$ = 2000 Hz (approx.)), 6.82 (br, $\Delta\nu_{1/2}$ = 650 Hz (approx.)), 2.06 (br, $\Delta\nu_{1/2}$ = 250 Hz (approx.)).
The broad and overlapping signals between 0–10 ppm precluded assignment.
Magnetic susceptibility (Evans method) μ_{eff} = 2.23 μ_B
EPR spectrum simulated with g_x = 2.065, g_y = 2.145, g_z = 2.519. lineshape = 0.95. The continuous wave X-band EPR spectrum was obtained at 9.390 GHz.

A small amount of **1-Br** is visible as a shoulder on the right-hand side of g_z in the black **3** spectrum (measured).

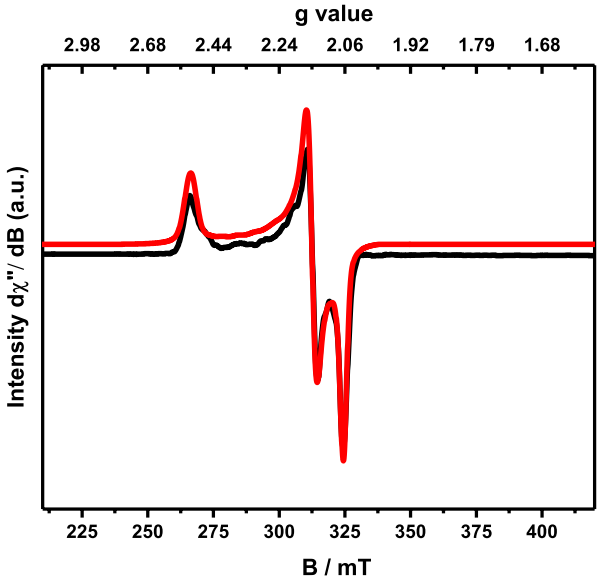

Figure S5. EPR spectrum of isolated 3 (77 K, 2-MeTHF). red = simulated spectrum.

In situ synthesis of Nickel(I)-alkyl complexes

[(L1)Ni(CH$_2$*t*Bu)] (3)

1-Br (5.0 mg, 0.0098 mmol, 1 equiv) was suspended in 1 mL 2-MeTHF. A solution of neopentylMgBr (145 µL, 0.029 mmol, 3 equiv) was then added and the vial agitated briefly to ensure reaction of the **1-Br**. The resulting deep green **3** solution was transferred to an EPR tube.

EPR spectrum simulated with $g_x = 2.065$, $g_y = 2.145$, $g_z = 2.519$. lineshape = 0.95. The continuous wave X-band EPR spectrum was obtained at 9.385 GHz.

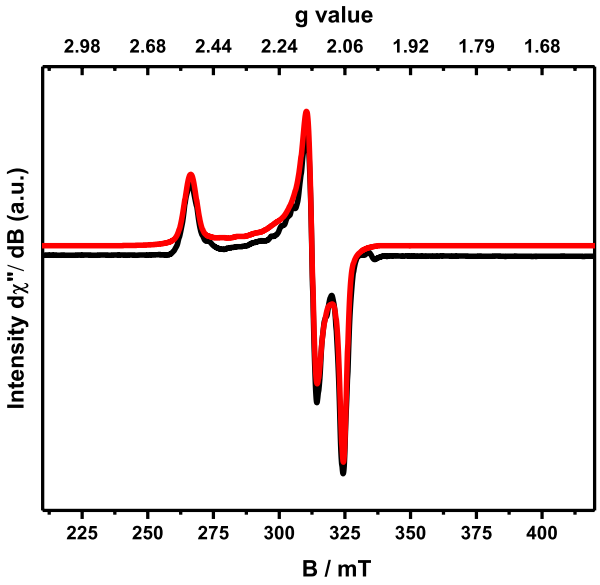

Figure S6. EPR spectrum of in situ generated 3 (77 K, 2-MeTHF).

The reaction was repeated and integration of the resulting EPR spectrum against solutions of known Cu(II) concentration gave a 68% yield of **3**:

1-Br (3.5 mg, 0.0055 mmol, 1 equiv) was suspended in 1 mL 2-MeTHF and cooled for 10 minutes in the freezer (−35 ºC). A solution of neopentylMgBr (35.75 µL, 0.0072 mmol, 1.3 equiv) was then added and the vial agitated for 5 minutes at room temperature to ensure reaction of the **1-Br**. The resulting deep green **3** solution was transferred to an EPR tube.

[(L2)Ni(CH$_2$*t*Bu)] (4)

2-Br (3.5 mg, 0.0055 mmol, 1 equiv) was suspended in 1 mL 2-MeTHF and cooled for 30 minutes in cold well of the glove box (< −100 ºC). A solution of neopentylMgBr (81 µL, 0.016 mmol, 3 equiv) was then added, the vial agitated briefly, then the deep green solution was transferred to a chilled EPR tube placed inside an aluminium block that had been kept in the cold well. This was removed from the glovebox then the tube frozen in liquid nitrogen.

EPR spectrum in Figure S7 simulated with $g_x = 2.074$, $g_y = 2.138$, $g_z = 2.506$. lineshape = 1. The continuous wave X-band EPR spectrum was obtained at 9.385 GHz.

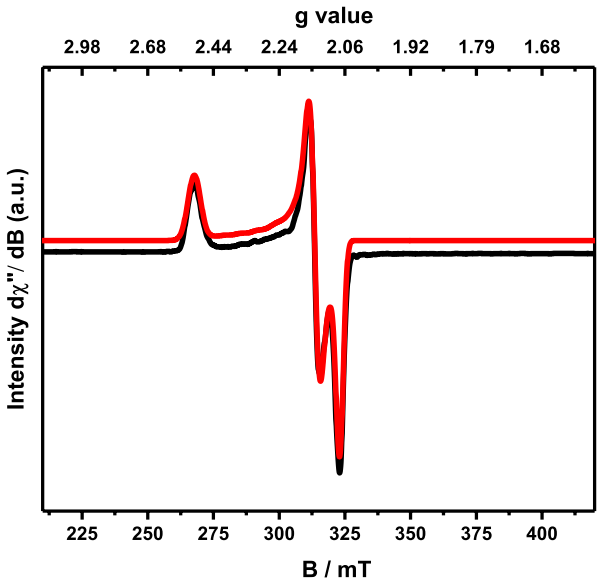

Figure S7. EPR spectrum of in situ generated 4 (77 K, 2-MeTHF). red = simulated spectrum.

The reaction was repeated and integration of the resulting EPR spectrum against solutions of known Cu(II) concentration gave a 57% yield of **4**:

2-Br (3.0 mg, 0.0055 mmol, 1 equiv) was suspended in 1 mL 2-MeTHF and cooled for 30 minutes in cold well of the glove box (< −100 ºC). A solution of neopentylMgBr (82.5 µL, 0.017 mmol, 3 equiv) was then added, the vial agitated briefly, then the deep green solution was transferred to a chilled EPR tube placed inside an aluminium block that had been kept in the cold well. This was removed from the glovebox then the tube frozen in liquid nitrogen.

Unsuccessful alkylation reactions of 1-Cl and 1-Br

Reactions between **L1** halide complexes **1-Cl** and **1-Br** and MeMgCl or EtMgBr were carried out as for the **2-Br** alkylation reactions described above. The resulting EPR spectra (77 K, 2-MeTHF glass) are shown below.

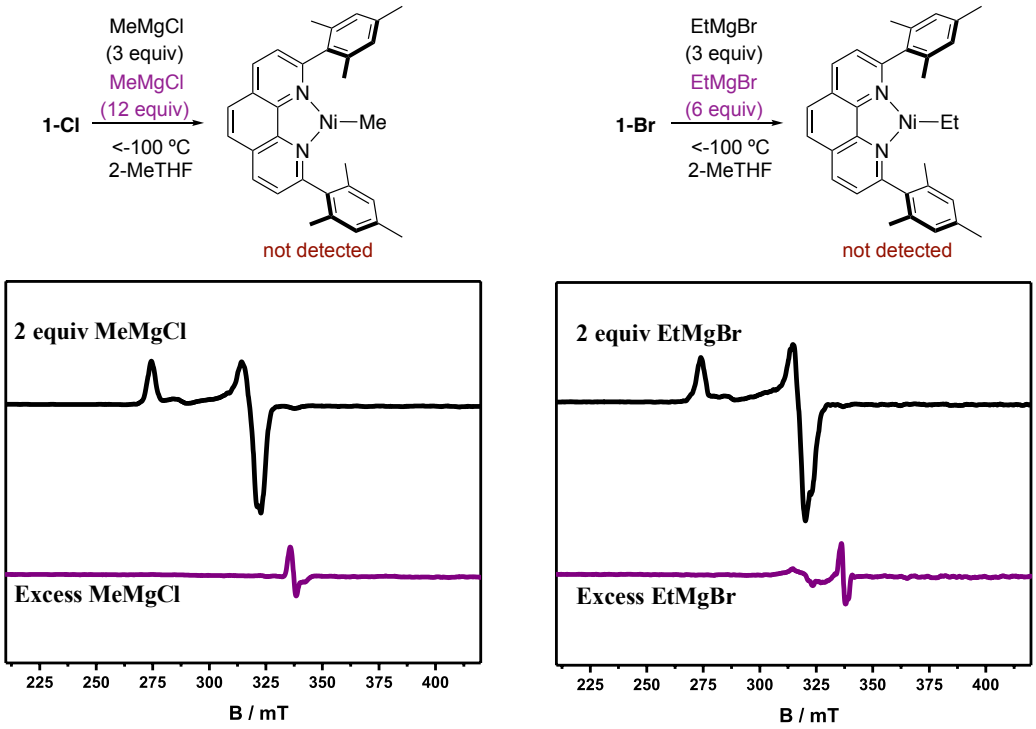

Figure S8. EPR spectra (77 K, 2-MeTHF) of reactions between [(L1NiX] and MeMgCl (left) and EtMgBr (right).

When the reaction of **1-Cl** with 2 equiv MeMgCl was carried out in toluene-d_8 and analysed by ^{1}H NMR spectroscopy, no clear paramagnetic signals could be identified. However, block-shaped green crystals were obtained. The crystals diffracted very poorly but the connectivity structure showed a [Ni(**L1**)]$_4$ tetramer (Figure S9). The Ni(**L1**) units coordinated to each C5–C6 bond of **L1** of another Ni(**L1**) unit.

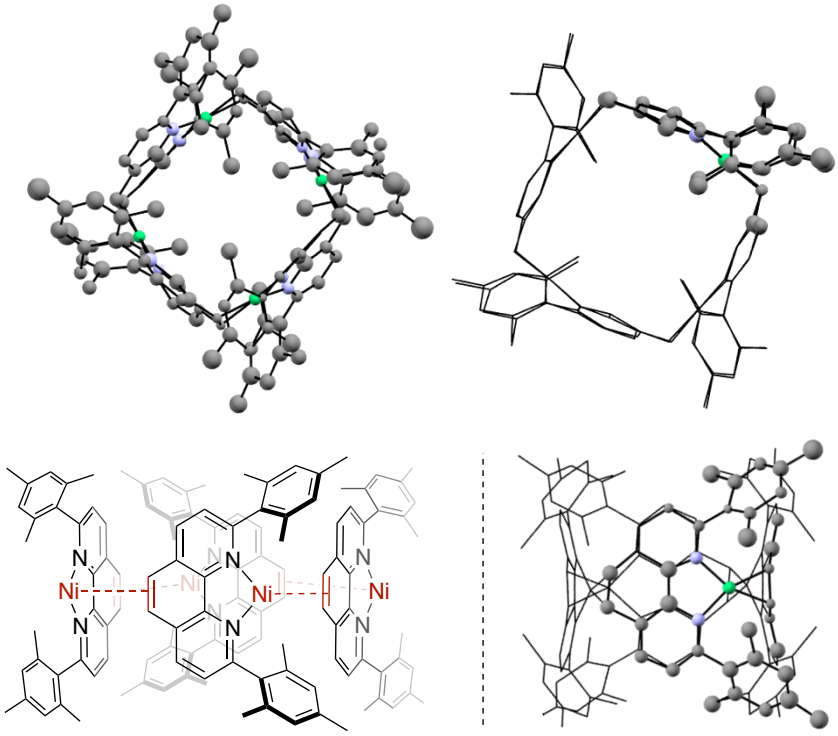

Figure S9. Connectivity structure of [Ni(L1)]$_4$ tetramer (two molecules in the asymmetric unit).

When **1-Br** was reacted with EtMgBr in THF-d$_8$, green crystals formed inside the NMR tube. A [Ni(**L1**)]$_3$ trimer structure was identified (Figure S10). Again, the crystals did not diffract well.

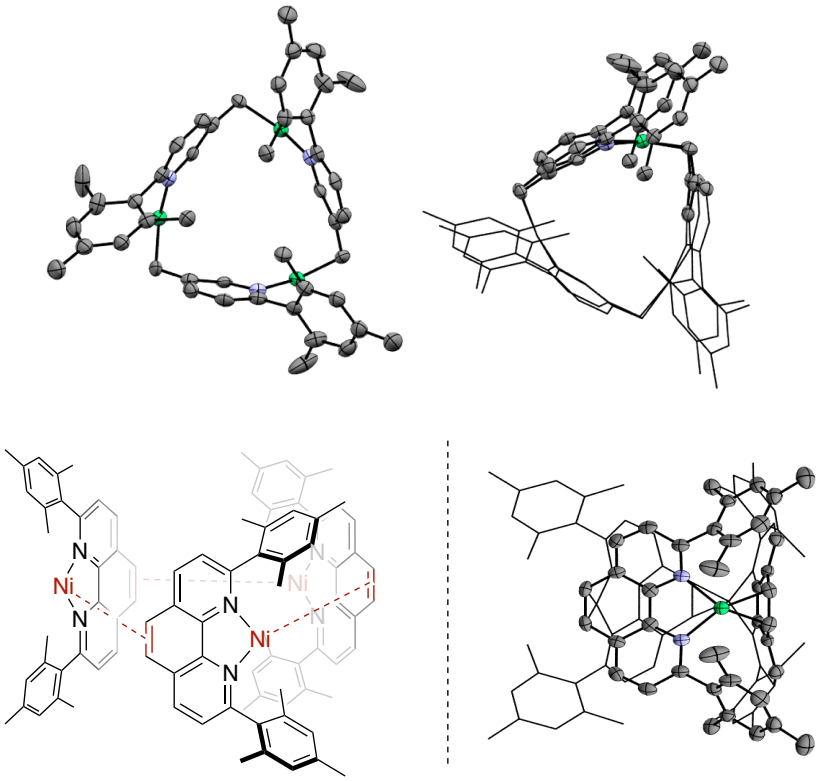

Figure S10. [Ni(L1)]$_3$. Hydrogen atoms and two THF molecules of crystallisation not shown.

There are no examples in the Cambridge Structural Database (as of March 2020) of complexes where the metal coordinates to the C5–C6 position of a phenanthroline ligand. The angle between (**L1**)Ni and the **L1** backbone to which it is coordinated is approximately 105º, consistent with reported complexes where a $L_nNi(0)$ group is coordinated to a π system.[8–12] The concavity of the **L1** backbone in both structures is unusual, however, and suggests that the phenanthroline ligand has lost aromaticity and is acting as two pyridine ligands separated by a π-bond spacer (where Ni(**L1**) coordinates) (Figure S11). The steric bulk of **L1** likely prevents formation of Ni(**L1**)$_2$, so this unusual interaction may be stabilising Ni(0) formed upon decomposition or reduction.

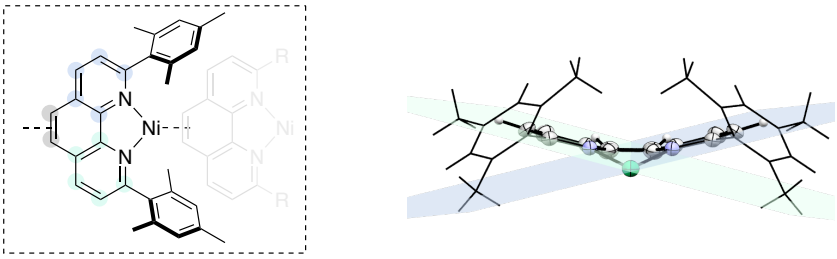

Figure S11. Fragment of [Ni(L1)]$_3$ to illustrate angle between planes (ca. 23°).

Nickel(I) carboxylate complex

Synthesis of 5 via anion metathesis

2-MeTHF:

1-Cl (6.2 mg, 0.012 mmol, 1 equiv) and KO_2CCH_2tBu (3.74 mg, 0.024 mmol, 2 equiv) were suspended in 2-MeTHF (1 mL) and stirred at room temperature for 30 minutes. After this time, a 0.4 mL aliquot was transferred to an EPR tube. The tube was sealed, taken out of the glovebox and the sample frozen in liquid nitrogen for analysis by EPR spectroscopy (77 K). NOTE: When the same reaction was repeated with 3 equiv KO_2CCH_2tBu (45 min) or with 1.5 equiv KO_2CCH_2tBu for 90 min, the resulting EPR signal for **5** was lower in intensity than that of the 2 equiv/30 min reaction.

Toluene:

1-Cl (6.2 mg, 0.012 mmol, 1 equiv) and KO_2CCH_2tBu (2.4 mg, 0.0156 mmol, 1.3 equiv) were suspended in toluene (1 mL) and stirred at room temperature for 5 minutes. After this time, a 0.4 mL aliquot was transferred to an EPR tube. The tube was sealed, taken out of the glovebox and the sample frozen in liquid nitrogen for analysis by EPR spectroscopy (77 K). One reaction was carried out in toluene-d_8 (0.7 mL) and after stirring for 5 minutes at room temperature, the solution was filtered through glass fibre filter paper and transferred to a J Young NMR tube in order to record the ^{1}H NMR spectrum.

For reactions where the IR spectrum was to be measured, only 1 equiv of KO_2CCH_2tBu was employed.

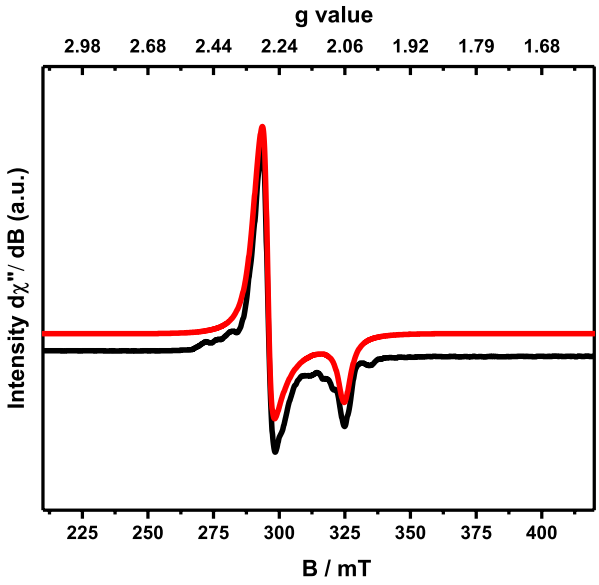

Figure S12. EPR spectrum of carboxylate complex 5 synthesised by anion metathesis. Simulated spectrum shown in red with: g_x = 2.299, g_y = 2.272, g_z = 2.064 freq: 9.388 GHz. lineshape = 0.

CO_2 insertion into Nickel(I)–alkyl complexes

Neopentyl complexes were either generated in situ with 1 equiv neopentylMgBr or isolated **3** was employed. An EPR spectrum of the neopentyl complex was always collected prior to CO_2 addition. Reactions involving **L2** neopentyl complexes were maintained at low temperature by working in the glovebox cold well and transferring the EPR tube from the glovebox while it was inside a cold aluminium block.

Procedure for CO_2 addition – small scale

The desired alkyl complex was dissolved in 2-MeTHF or prepared from the appropriate [(**L**)NiBr] complex and neopentylMgBr inside the glovebox. The solution was then transferred to a resealable EPR tube and frozen in liquid N_2. The atmosphere in the tube was carefully exchanged for 0.1 bar CO_2, then the reaction mixture was thawed to ca. −60 ºC (ethanol dry ice bath, thermometer), briefly agitated, and finally refrozen under vacuum.

Addition of $^{13}CO_2$ was carried out in a similar manner using a 1 L lecture bottle (Sigma Aldrich). Pressure inside the (new) bottle was 1.36 atm.

Procedure for CO_2 addition – quenching experiments

For larger scale experiments (Scheme 3 in manuscript), a teflon-sealed Schlenk ampoule containing an Et_2O solution of the appropriate [(**L**)NiBr] complex (generated in situ from **1-Br** or **2-Br** and neopentylMgBr at room temperature and in the cold well of the glovebox, respectively) was frozen, placed under vacuum, then warmed slightly prior to CO_2 addition to avoid condensing CO_2 (e.g. to –60 °C for reaction shown below). The solution was then warmed to room temperature and agitated for 15 minutes. Afterwards, the reaction was quenched with 2M HCl and the Et_2O layer was extracted. A ^{1}H NMR spectrum was recorded using TMS or 1,3,5-trimethoxybenzene as internal standard.

2-Br (43 mg, 0.067 mmol, 1 equiv) was weighed into a Schlenk ampoule then suspended in Et_2O and cooled in an aluminium block placed in the liquid N_2-cooled cold well of the glovebox. After 30 minutes, neopentylMgBr (336 µL, 0.067 mmol, 1 equiv) was added dropwise, resulting in a color change to green. The reaction vessel was removed periodically from the cold well and agitated until all the blue solid **2-Br** seemed to have reacted. The Schlenk was then removed from the glovebox while still in the cold aluminium block, then the procedure to add CO_2 described above was followed.

Catalytic carboxylation reactions

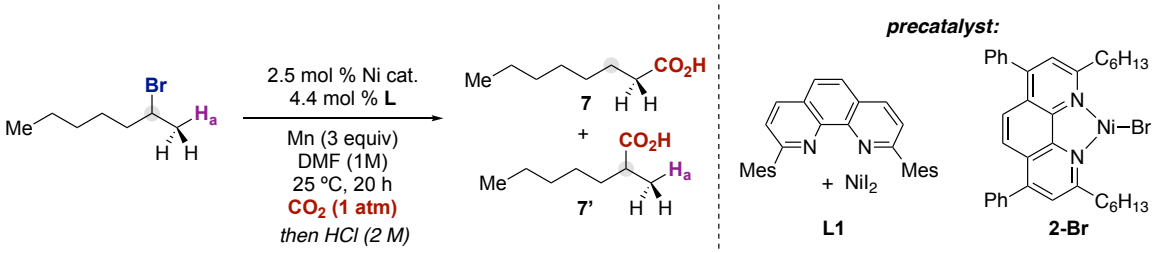

Scheme S2. General scheme for investigating the catalytic ability of 2-Br and L1 complexes.

Following a reported literature procedure:[4]

An oven-dried teflon-sealed Schlenk ampoule containing a stirring bar was charged with the corresponding Ni source, ligand, and Mn powder reducing agent. If the Ni source was to be [(**L2**)NiBr] (**2-Br**), the Schlenk tube was then taken into the glovebox where the **2-Br** was added. Outside the glovebox, the Schlenk tube was evacuated and back-filled under a flow of carbon dioxide (this sequence was repeated three times) then placed under 1 atm CO_2. The solvent and 2-bromoheptane (0.50 mmol) were subsequently added by syringe, then the Schlenk tube was sealed and the solution taken to the corresponding temperature and stirred for 20 h. After this time, the mixture was allowed to equilibrate with room temperature, carefully quenched with 2 M HCl to hydrolyze the resulting Mn-carboxylate, and finally extracted with EtOAc. A sample of the organic layer was analyzed by GC.

Table S1. Screening of 2-Br and L1 complexes in the chain-walking carboxylation of 2-bromoheptane.

Entry	Ni catalyst	**L**	Conversion (%)[a]	**7** (%)[a]	Ratio **7**:**7'** [a]
1	NiI_2	**L2**	94	76	98:2
2	NiI_2	**L1**	100	33	99:1
3	[(**L2**)NiBr] (**2-Br**)[b]	**L2**	100	49	97:3

Reaction conditions: 2-bromoheptane (0.50 mmol, 1 equiv), Ni catalyst (2.5 mol %), **L** (4.4 mol %), Mn (1.50 mmol, 3.0 equiv.), CO_2 (1 atm) in DMF (1 M) at 25 ºC for 20 h. [a]Yields and linear/branched ratio were determined by GC FID using anisole as internal standard. [b]When using **2-Br** as precatalyst, 1.9 mol % of **L2** was used instead of 4.4 mol %.

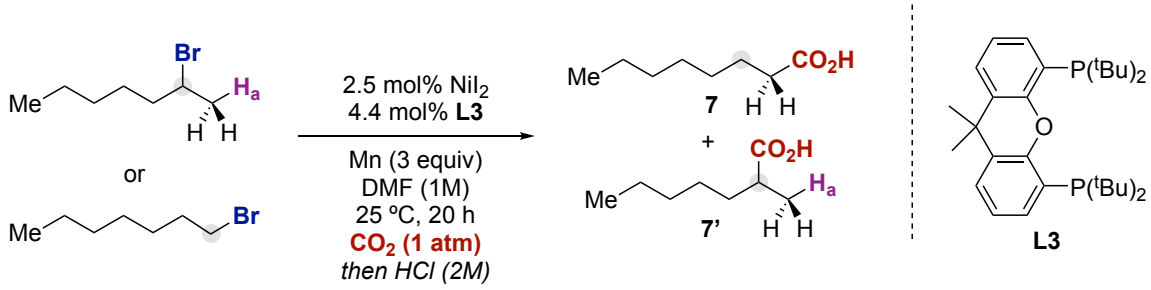

Scheme S3. General scheme for investigating the catalytic ability of L3.

Following a reported literature procedure:[4]

An oven-dried teflon-sealed Schlenk ampoule containing a stirring bar was charged with the corresponding Ni source, ligand, and Mn powder reducing agent. The Schlenk was evacuated and back-filled under a flow of carbon dioxide (this sequence was repeated three times) then placed under 1 atm CO_2. The solvent and 2-bromoheptane (0.50 mmol) or 1-bromoheptane (0.50 mmol) were subsequently added by syringe, then the Schlenk tube was sealed and the solution taken to the corresponding temperature and stirred for 20 h. After this time, the mixture was allowed to equilibrate with room temperature, carefully quenched with 2 M HCl to hydrolyze the resulting Mn-carboxylate, and finally extracted with EtOAc. A sample of the organic layer was analyzed by GC.

Table S2. Screening of L3 in the chain-walking carboxylation of 2-bromoheptane and 1-bromoheptane.

Entry	Substrate	Conversion (%)[a]	**7** (%)[a]	Ratio **7**:**7'** [a]
1	2-bromoheptane	2	0	-
2	1-bromoheptane	1	0	-

Reaction conditions: 1- or 2-bromoheptane (0.50 mmol, 1 equiv), NiI_2 (2.5 mol %), **L3** (4.4 mol %), Mn (1.50 mmol, 3.0 equiv.), CO_2 (1 atm) in DMF (1 M) at 25 ºC for 20 h. [a]Yields and linear/branched ratio were determined by GC FID using anisole as internal standard.

IR spectra

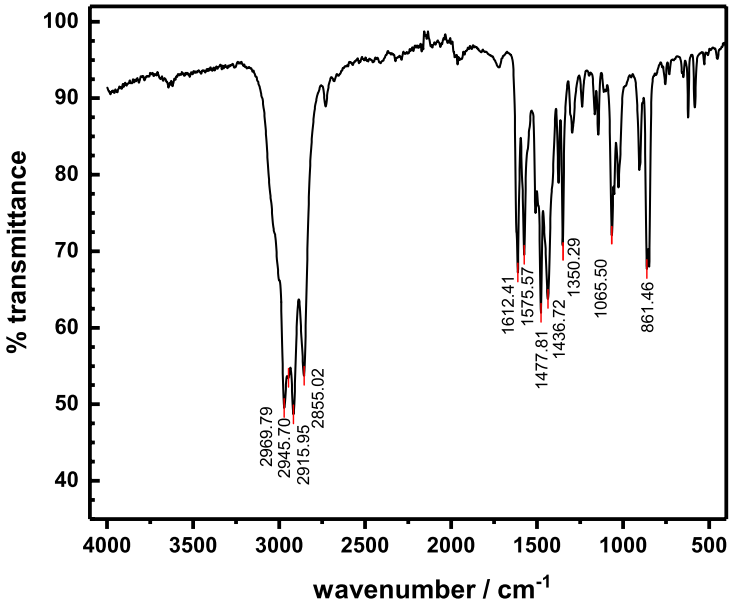

Figure S13. IR spectrum of 1-Br.

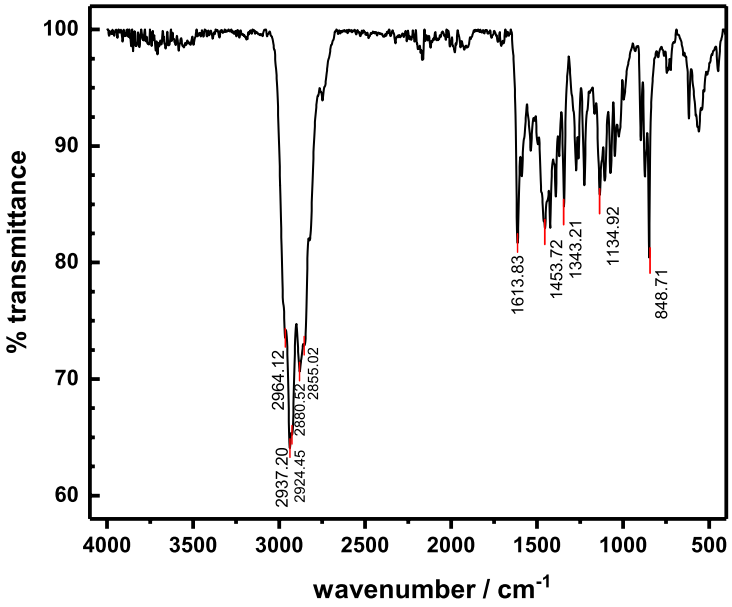

Figure S14. IR spectrum of 3.

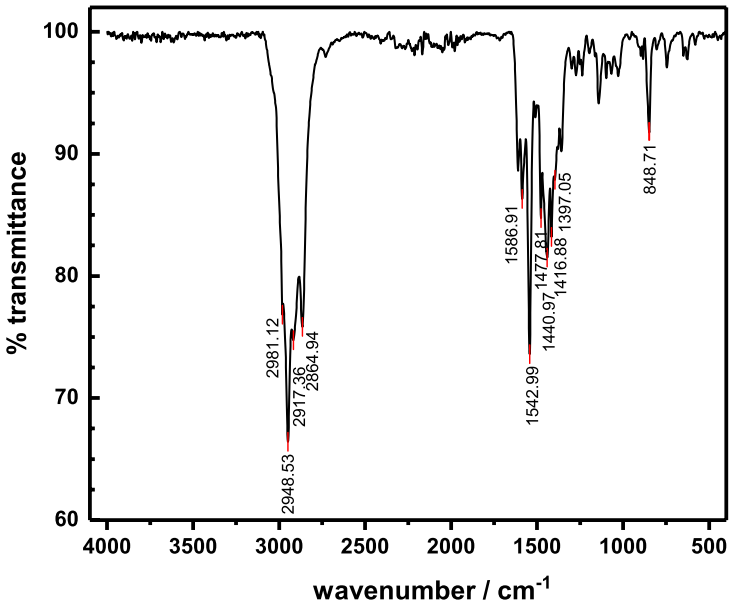

Figure S15. IR spectrum of anion metathesis product (5).

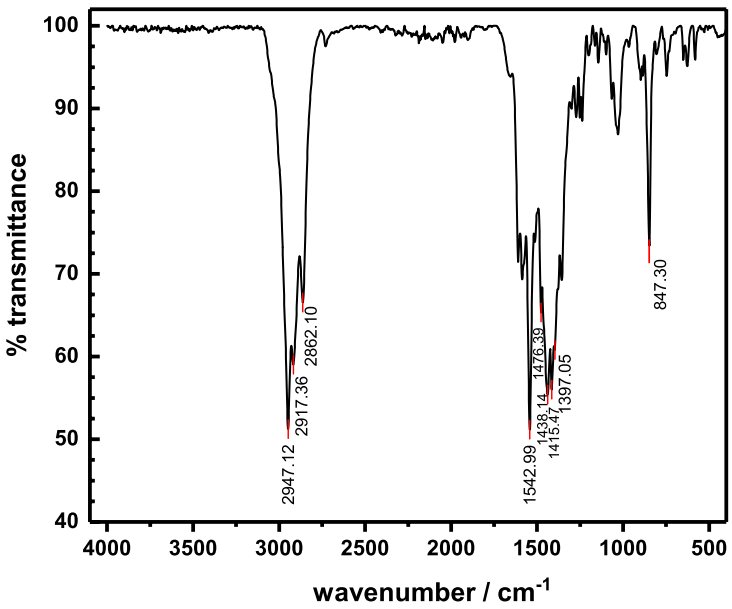

Figure S16. IR spectrum of CO_2 insertion to 3.

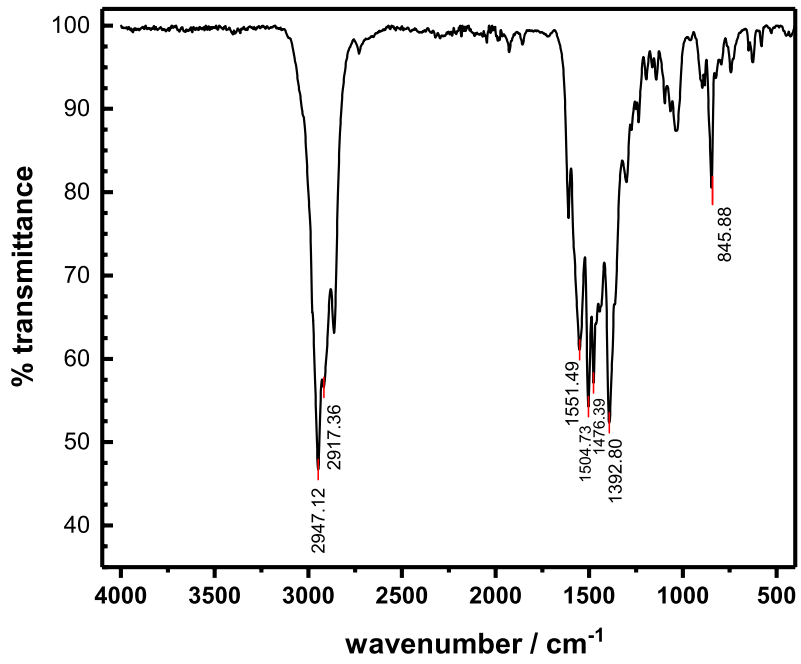

Figure S17. IR spectrum of $^{13}CO_2$ insertion to 3.

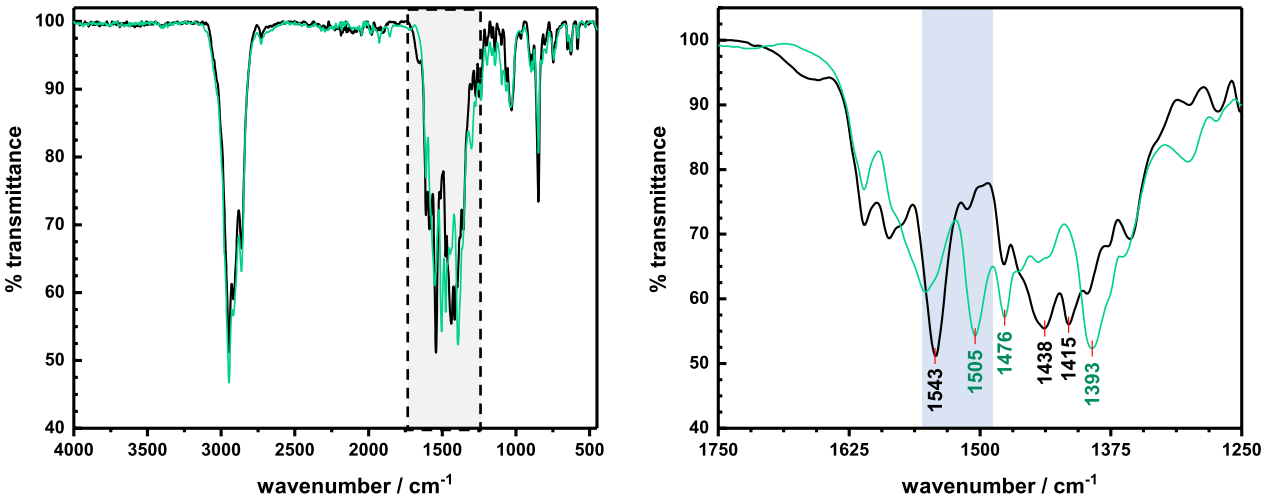

Figure S18. Overlay of IR spectra of CO_2/$^{13}CO_2$ (black/green) insertion to 3.

NMR data of halide complexes

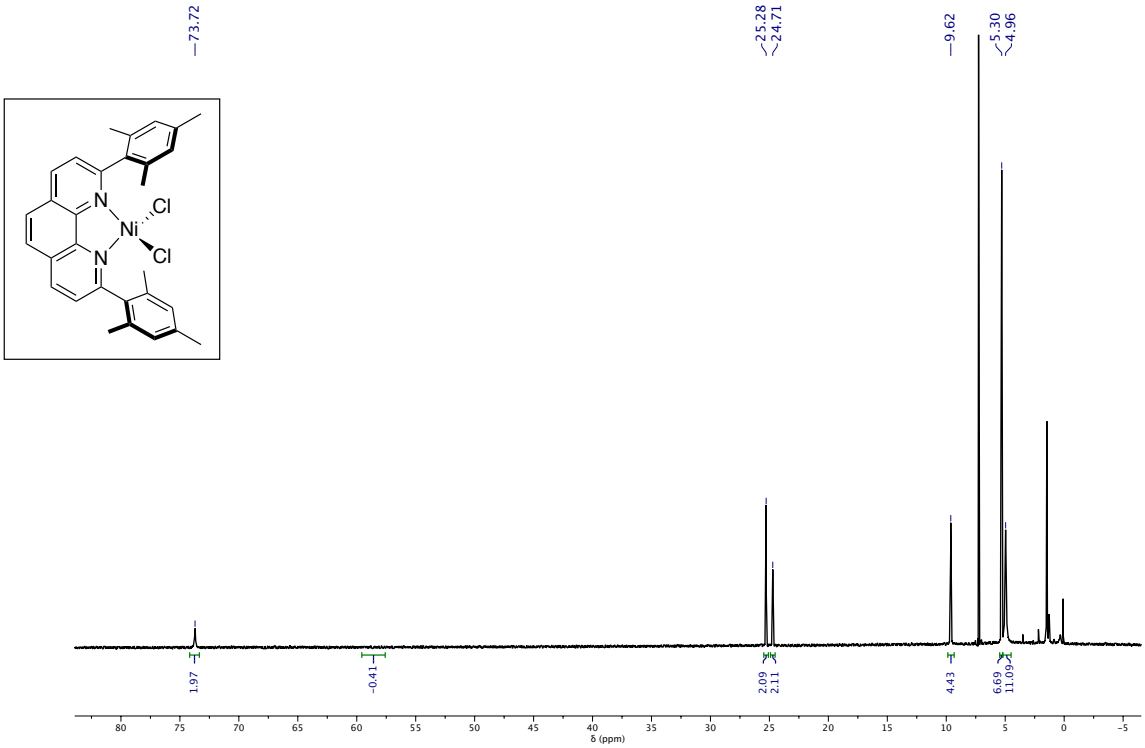

Figure S19. ^{1}H NMR (500 MHz, $CDCl_3$) of [$NiCl_2$(L1)].

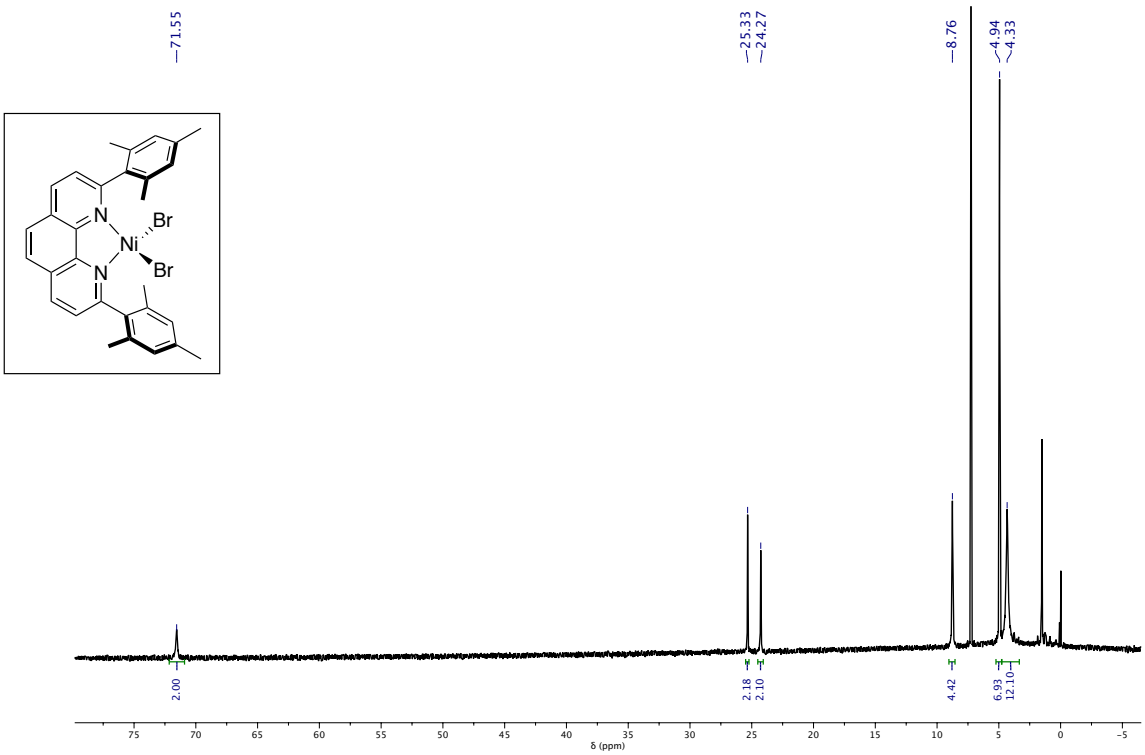

Figure S20. ^{1}H NMR (500 MHz, $CDCl_3$) of [$NiBr_2$(L1)].

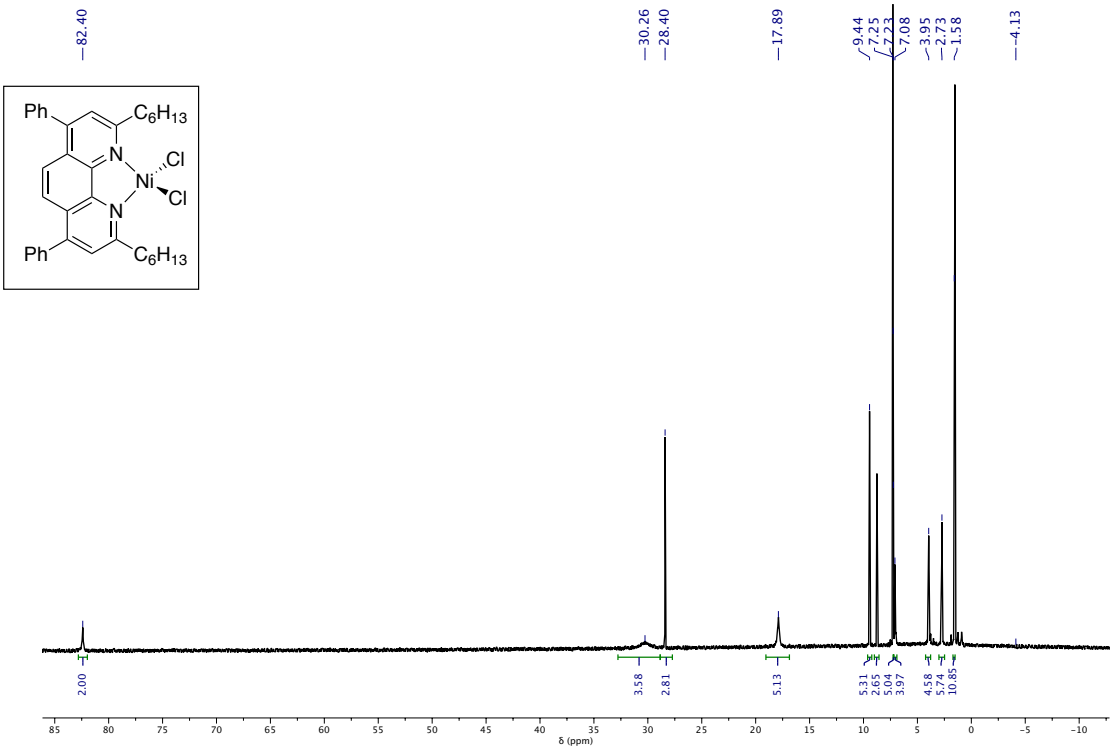

Figure S21. ^{1}H NMR (400 MHz, $CDCl_3$) of [$NiCl_2$(L2)].

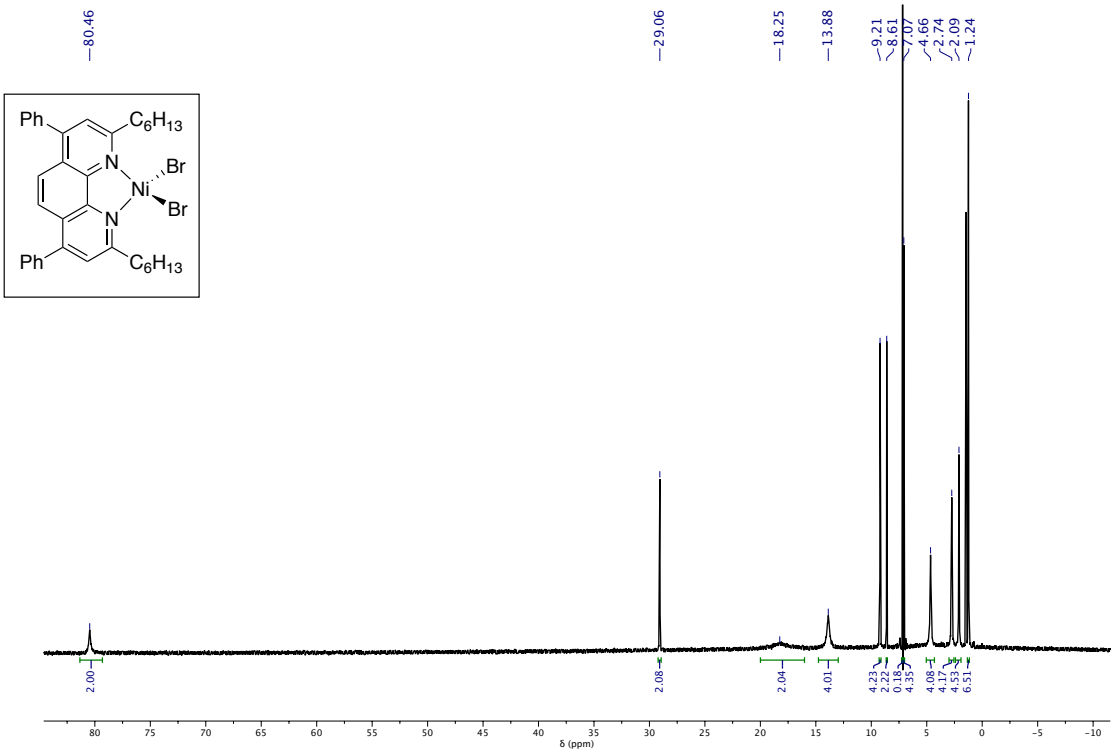

Figure S22. ^{1}H NMR (400 MHz, $CDCl_3$) of [$NiBr_2$(L2)].

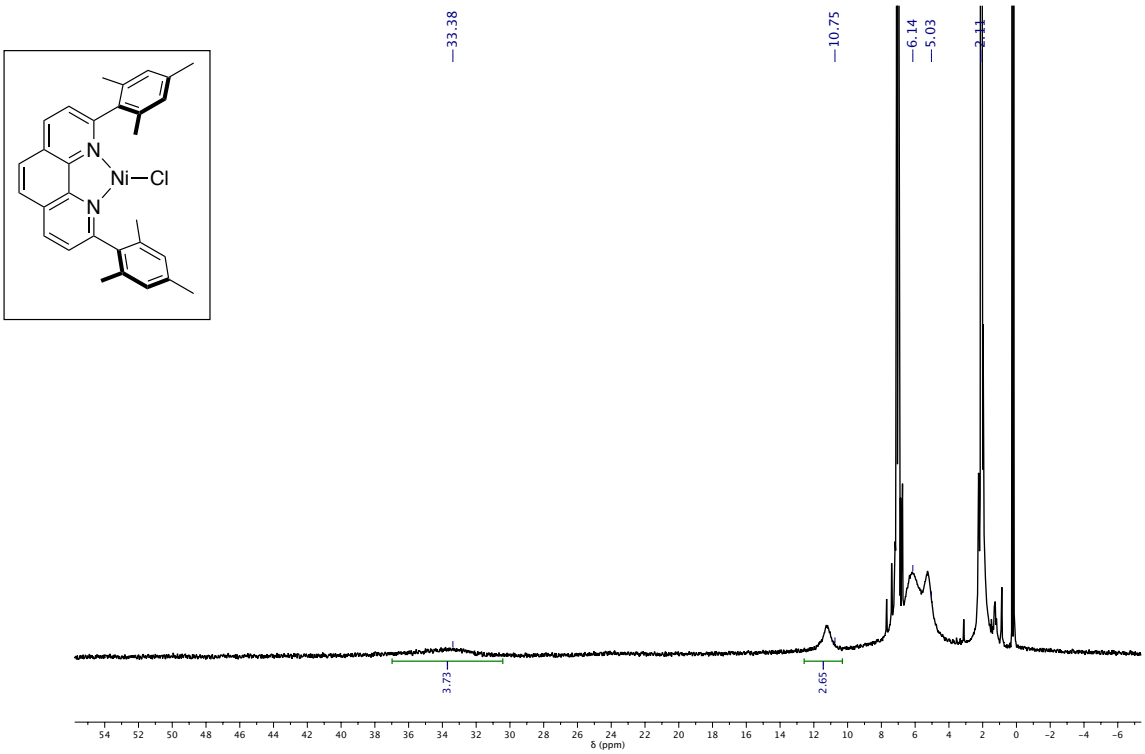

Figure S23. ^{1}H NMR (500 MHz, toluene-d$_8$) of 1-Cl.

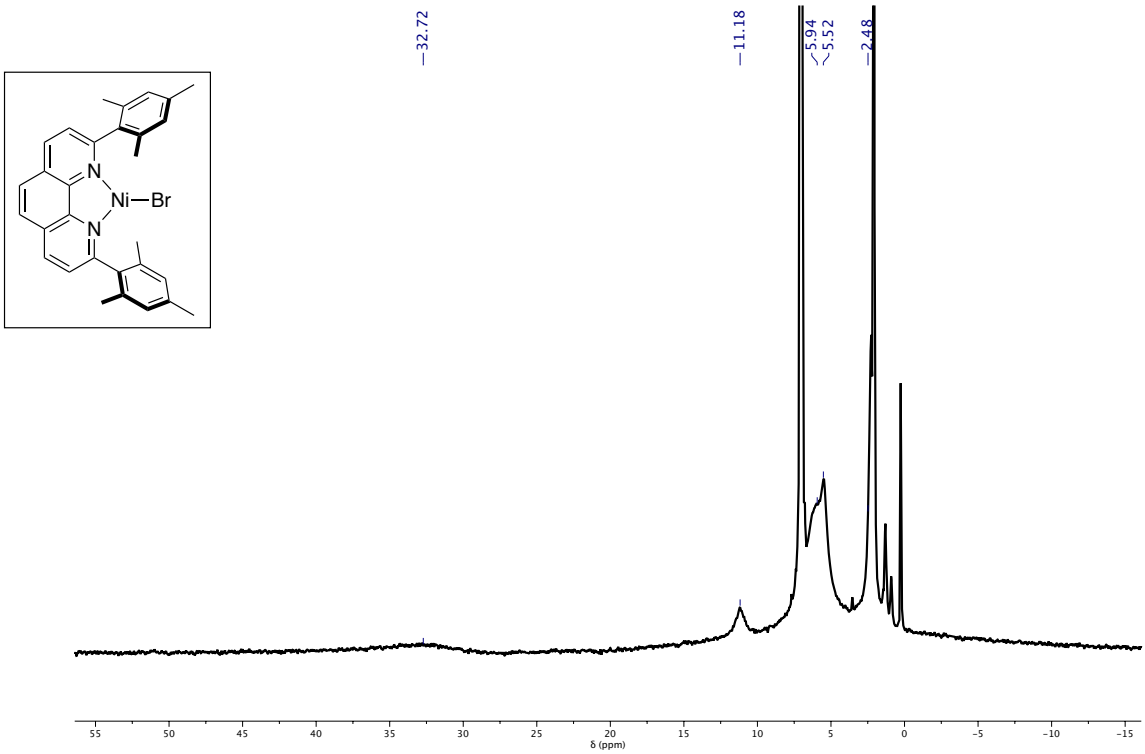

Figure S24. ^{1}H NMR (500 MHz, toluene-d$_8$) of 1-Br.

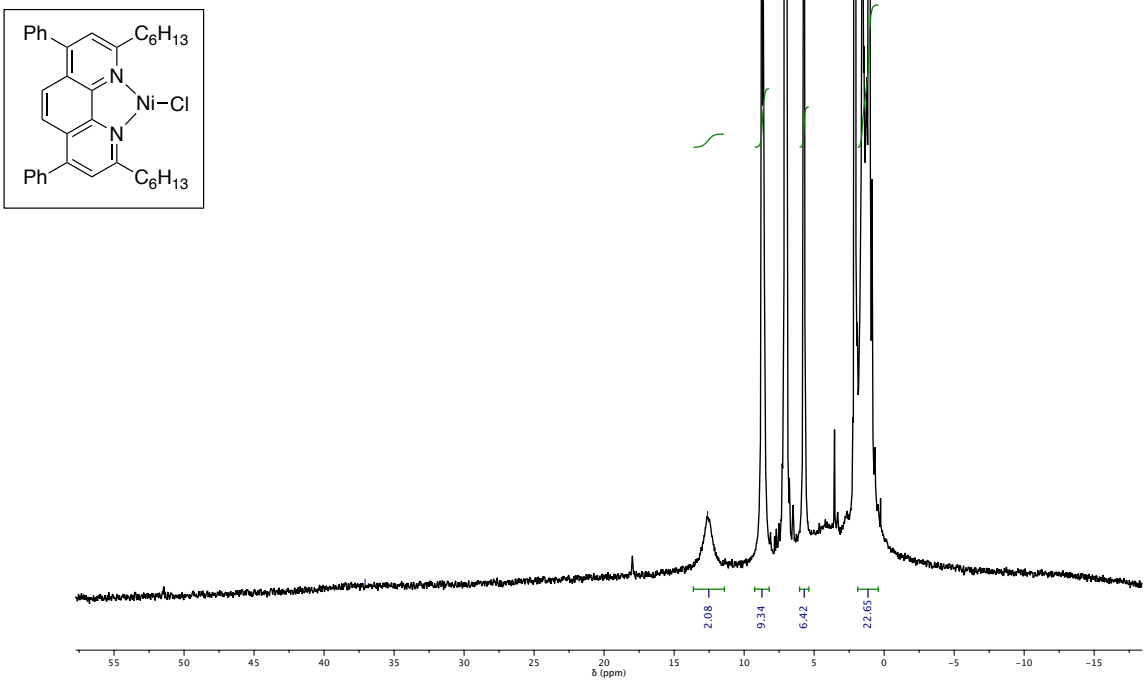

Figure S25. ^{1}H NMR (400 MHz, toluene-d$_8$) of 2-Cl.

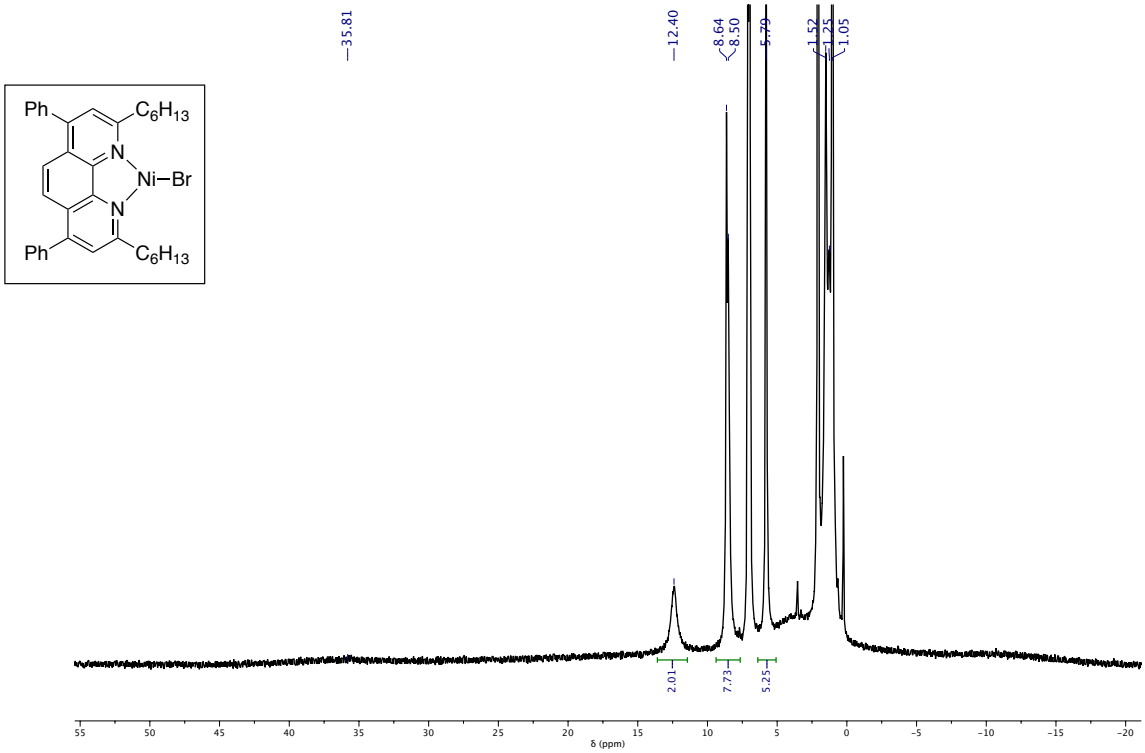

Figure S26. ^{1}H NMR (400 MHz, toluene-d$_8$) of 2-Br.

NMR data of alkyl complexes

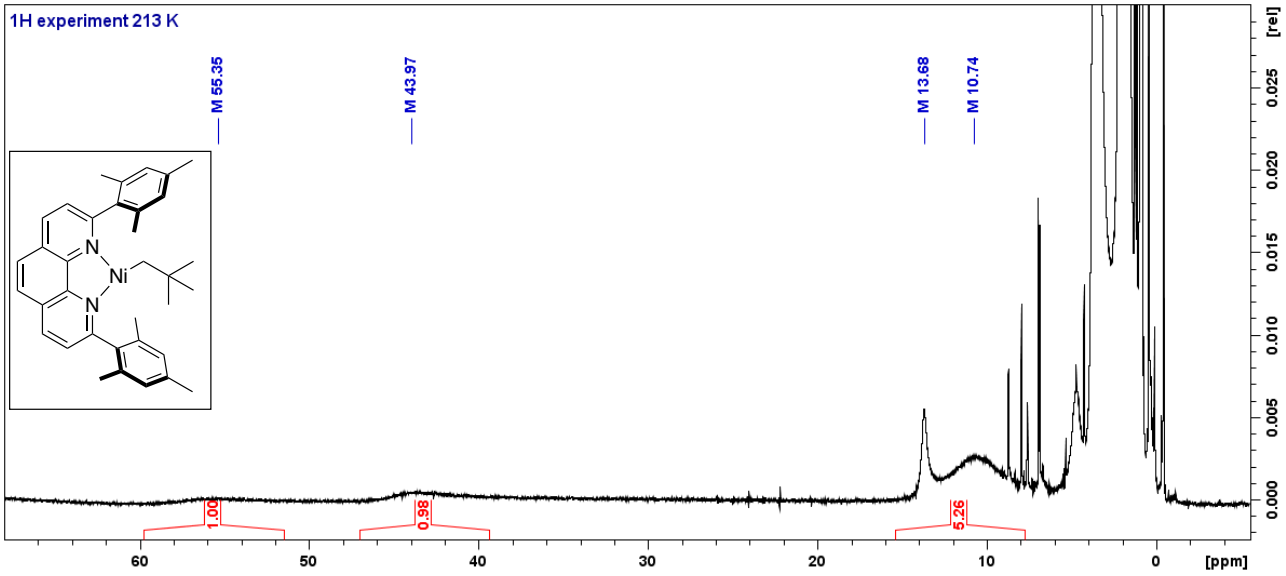

Figure S27. ^{1}H NMR (500 MHz, THF-d$_8$, 213 K) of 3.

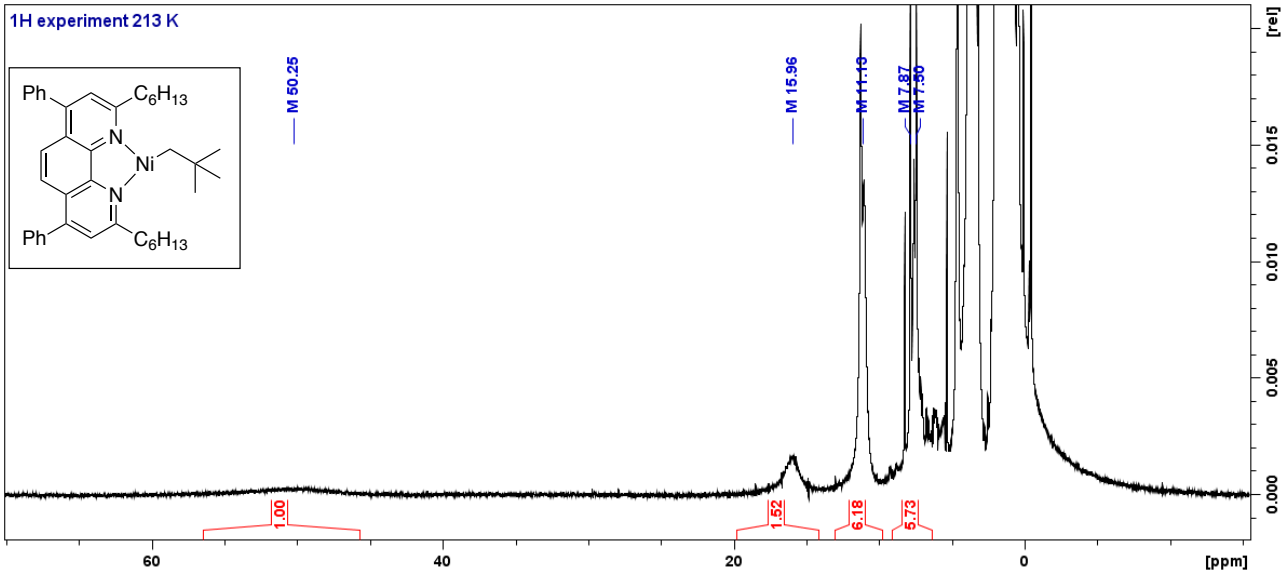

Figure S28. ^{1}H NMR (500 MHz, THF-d$_8$, 213 K) of 4.

NMR data of 5

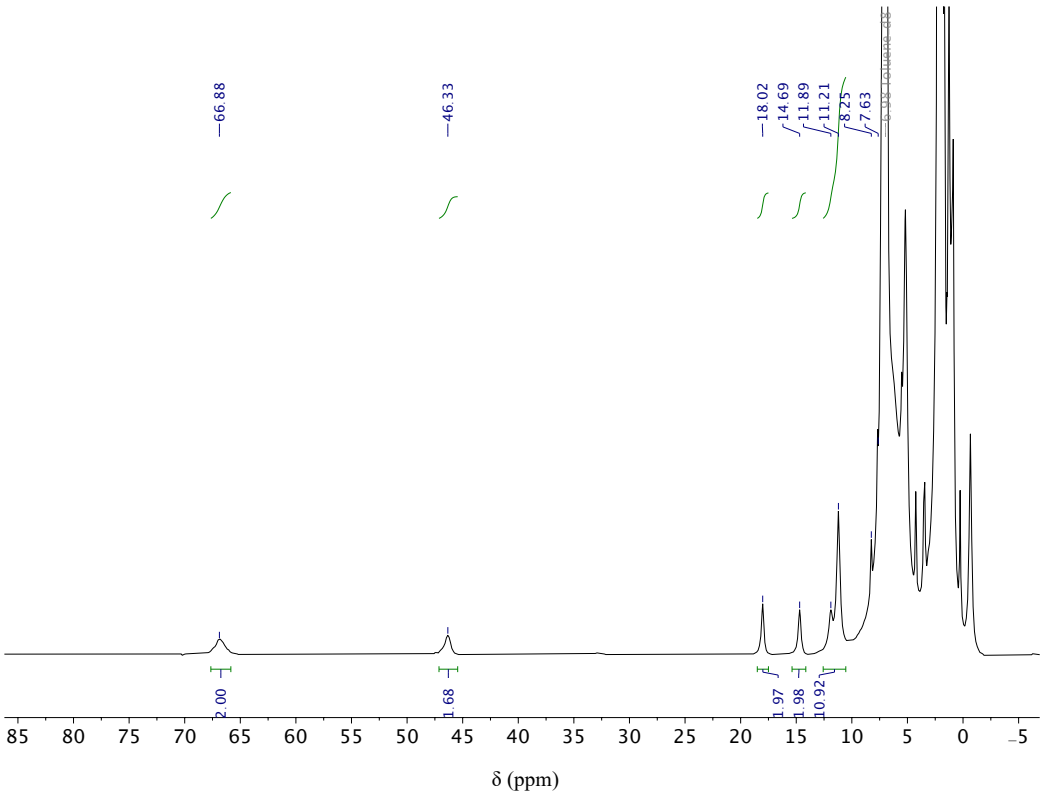

Figure S29. ^{1}H NMR (500 MHz, toluene-d$_8$, 213 K) of 5.

Crystallographic data

CCDC deposition numbers:
1-Cl: 1990525
2-Cl: 1990348
3: 1990349

Details for 1-Cl (Dr. Brandon Q. Mercado, Yale University)

Low-temperature diffraction data (ω-scans) were collected on a Rigaku MicroMax-007HF diffractometer coupled to a Dectris Pilatus3R detector with Mo Kα (λ = 0.71073 Å) for the structure of 007c-18081. The diffraction images were processed and scaled using Rigaku Oxford Diffraction software (CrysAlisPro; Rigaku OD: The Woodlands, TX, 2015). The structure was solved with SHELXT and was refined against F^2 on all data by full-matrix least squares with SHELXL (Sheldrick, G. M. Acta Cryst. 2008, A64, 112–122).

All non-hydrogen atoms were refined anisotropically. Hydrogen atoms were included in the model at geometrically calculated positions and refined using a riding model. The isotropic displacement parameters of all hydrogen atoms were fixed to 1.2 times the U value of the atoms to which they are linked (1.5 times for methyl groups). The program SQUEEZE was used to compensate for the contribution of disordered solvents contained in voids within the crystal lattice from the diffraction intensities. This procedure was applied to the data file and the submitted model is based on the solvent removed data. Based on the total electron density found in the voids (325 e/Å^3), it is likely that ~6.5 toluene molecules are present in the unit cell. See "_platon_squeeze_details" in the .cif for more information.

- Sheldrick, G. M. *SHELXTL* Version 2014/7. *http://shelx.uni-ac.gwdg.de/SHELX/index.php*

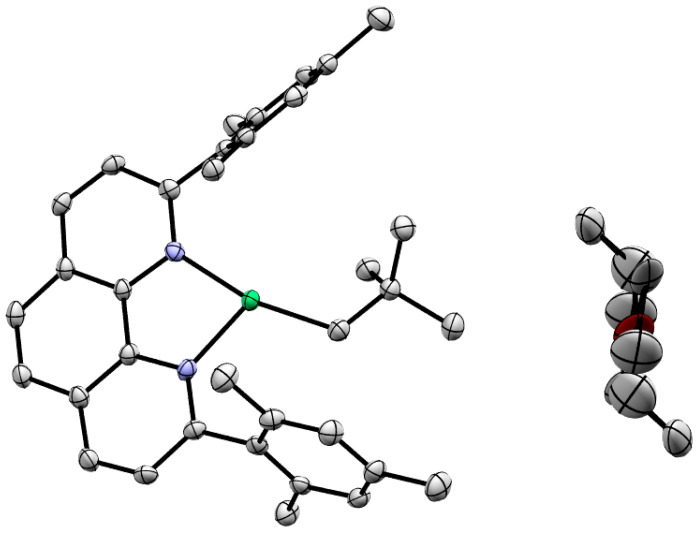

Figure S30. ORTEP diagram of 3 showing disordered solvent: one molecule of diethyl ether (reflected in data shown in Table S3.

Table S3. Crystallographic data.

	1-Cl	2-Cl	3
Formula	$C_{30}H_{28}ClN_2Ni$	$C_{36}H_{40}ClN_2Ni$	$C_{37}H_{44}N_2NiO_{0.5}$
Formula weight	510.70	594.86	583.45
T (K)	93(2)	100(2)	100(2)
Wavelength (Å)	0.71073	0.71073	0.71073
Crystal system	Triclinic	monoclinic	monoclinic
Space group	P-1	P 21/c	P 21/c
***a* (Å)**	18.0288(15)	9.8891(16)	11.0083(6)
***b* (Å)**	18.5080(14)	21.524(3)	32.4592(17)
***c* (Å)**	22.4157(15)	14.620(2)	8.8043(5)
α (deg)	113.701(7)	90	90
β (deg)	90.846(7)	103.029(5)	90.9405(18)
γ (deg)	114.996(8)	90	90
V (Å^3)	6051.7(9)	3031.8(8)	3145.5(3)
Z	8	4	4
Density (calcd.) (Mg/cm^{-3})	1.121	1.303	1.232
μ (mm^{-1})	0.747	0.755	0.646
F(000)	2136	1260	1248
Crystal size (mm^3)	0.200 x 0.150 x 0.070	0.200 x 0.050 x 0.050	0.300 x 0.050 x 0.020
Theta range for data collection (deg)	2.725 to 27.484	2.114 to 26.565	1.954 to 25.076
Index ranges	-21<=h<=23, -24<=k<=24, -28<=l<=29	-12<=h<=12, -26<=k<=26, -18<=l<=13	-12<=h<=13, -38<=k<=37, -10<=l<=8
Reflections collected	116021	19883	41144
Independent reflections	27570 [R(int) = 0.1214]	6057 [R(int) = 0.0687]	5508 [R(int) = 0.1016]
Completeness to theta	99.8% (25.242°)	95.5% (26.565º)	98.7% (25.076)
Absorption correction	Semi-empirical from equivalents	Multi-scan	Multi-scan
Max. and min. transmission	1.00000 and 0.49560	0.74 and 0.49	0.74 and 0.49
Refinement method	SHELXL-2014/7 (Sheldrick, 2014)	Full-matrix least-squares on F^2	Full-matrix least-squares on F^2
Data/restraints/parameters	27570/0/1249	6057/0/363	5508/61/399
Goodness-of-fit on F^2	0.986	1.032	1.055
Final R indices [I>2sigma(I)]	R1 = 0.0452, wR2 = 0.1058	R1 = 0.0526, wR2 = 0.1148	R1 = 0.0521, wR2 = 0.1090
R indices (all data)	R1 = 0.0799, wR2 = 0.1163	R1 = 0.0935, wR2 = 0.1306	R1 = 0.0821, wR2 = 0.1217
Largest diff. peak and hole	0.612 and −0.559 e.Å^{-3}	0.845 and −0.554 e.Å^{-3}	0.556 and -0.439 e.Å^{-3}

Computational Details

All calculations were performed on the full molecular models without any truncations using Gaussian16, Revision B.01.[13] Results in the main text correspond to the GGA functional PBE,[14,15] with additional results using the hybrid functional B3LYP[16] reported in the Supporting Information for comparison. Optimizations with both functionals were done in combination with the Grimme empirical dispersion correction with Becke-Johnson damping D3BJ[17] and the solvent model IEFPCM[18–20](THF). For all calculations, we employed the basis set def2-TZVP. Vibrational mode analysis was performed for all structures to ensure that they have zero (ground state) or exactly one (TS) imaginary frequency. Calculated IR spectra were obtained by utilizing the harmonic approximation, therefore, all obtained wavenumbers/frequencies were scaled according to the CCCBDB[21] (0.986 for PBE, 0.96 for B3LYP) to account for this. All optimized geometries are found in the accompanying .xyz file.

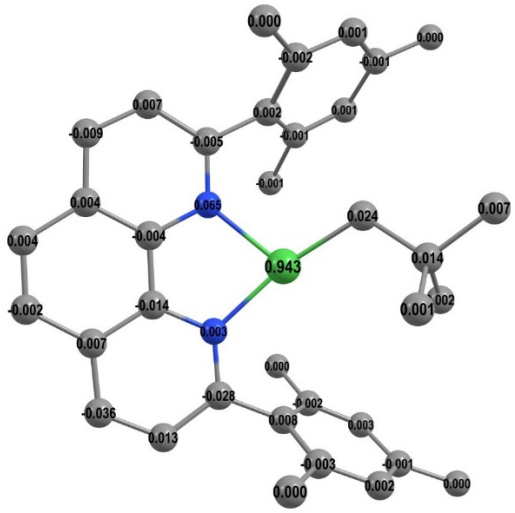

Figure S31. Calculated structure (PBE-D3BJ/def2-TZVP/IEFPCM(THF)) of **3** with the hydrogen atoms removed for clarity. Numbers are computed spin populations. Selected distances (Å) and angles (°): Ni–C 1.981 Å, N1–Ni–C1 159.5°, N2–Ni–C1 108.9°.

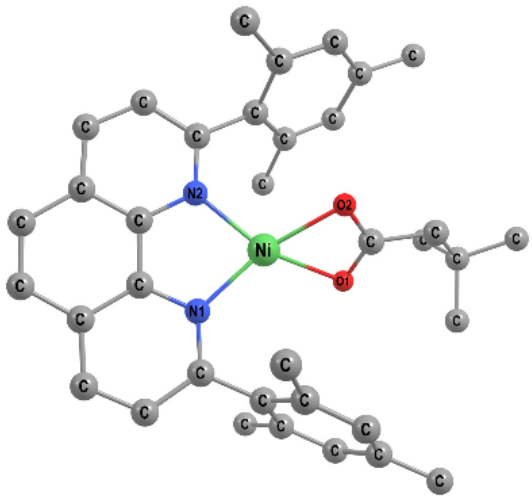

Figure S32. Calculated structure (PBE-D3BJ/def2-TZVP/IEFPCM(THF)) of **5** with the hydrogen atoms removed for clarity. Selected distances (Å) and angles (°): N1/2-Ni 1.99 Å , O1-Ni 2.12 Å , O2-Ni 2.14 Å , N1-Ni-N2 83.2°, O1-Ni-O2 62.6°, N1-Ni-O1 111.4°, N2-Ni-O2 116.5°.

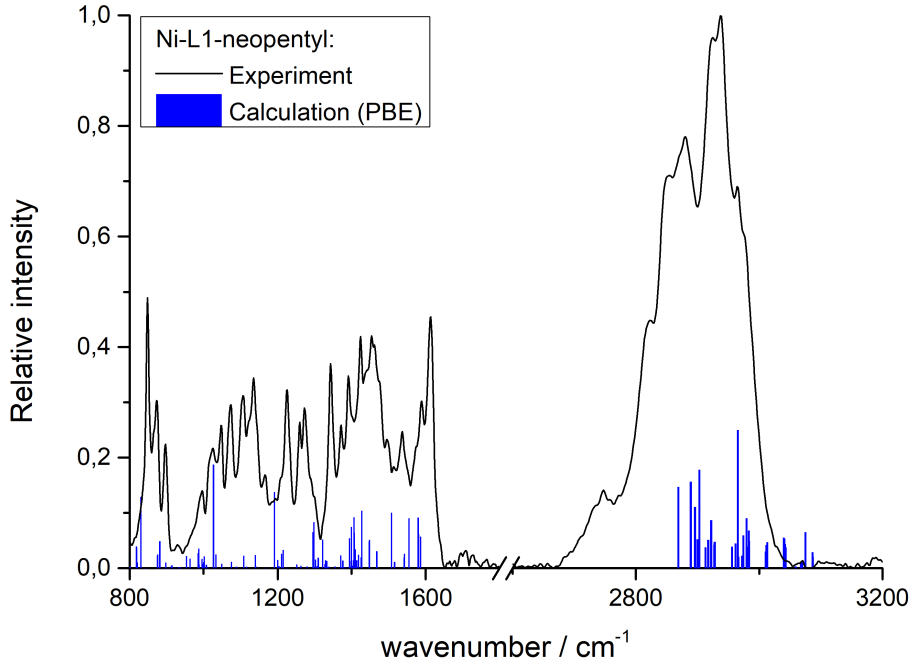

Figure S33. Comparison of the experimental (black) and calculated IR spectra (blue, PBE-D3BJ/def2-TZVP/IEFPCM(THF)) for **3**.

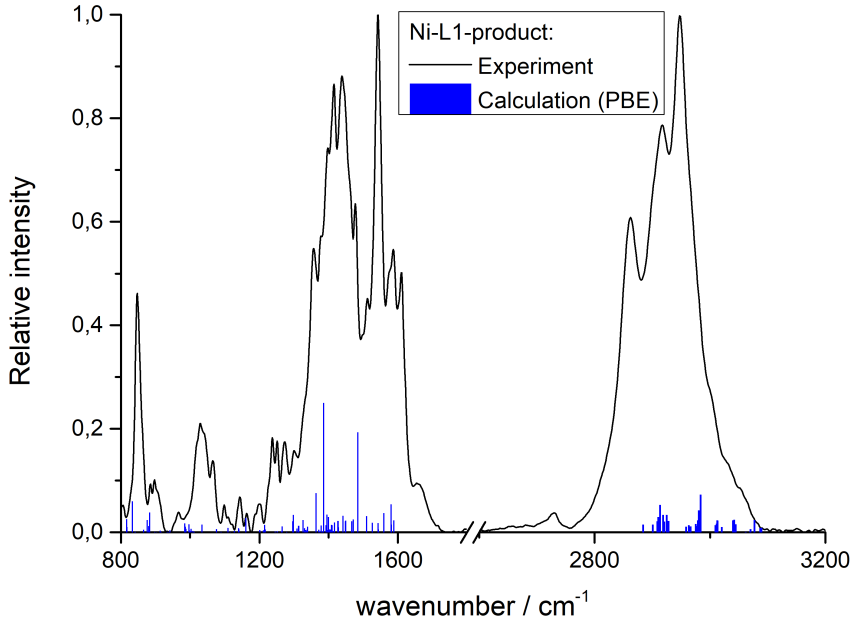

Figure S34. Comparison of experimental (black) and calculated IR spectra (blue, PBE-D3BJ/def2-TZVP/IEFPCM(THF)) for **5**.

The influence of replacing the carbon atom of the CO_2 with a ^{13}C atom was computed and predicted a shift of 34 cm^{-1} (1484−1450 cm^{-1}) (PBE-D3BJ) or 36 cm^{-1} (1503−1467 cm^{-1}) (B3LYP-D3BJ) towards lower wavenumbers.

This is similar to the experimentally observed shift from 1543 to 1505 cm^{-1} (Δ = 38 cm^{-1}) (see Figure S18) and supports the conclusion that **5** was synthesized.

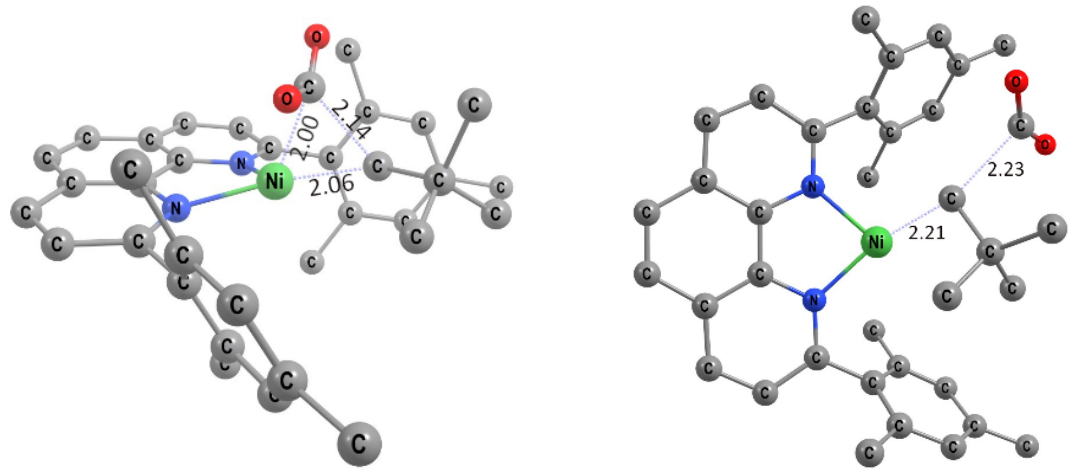

Figure S35. Optimized TS geometries of the inner (left, barrier 7.7 kcal/mol) and outer sphere (right, barrier 22.7 kcal/mol) CO_2 insertion into **3** (PBE-D3BJ/def2-TZVP/IEFPCM(THF)). Hydrogen atoms are removed for clarity. Distances are given in Å.

Table S4. Comparison of calculated Gibbs free energy barriers (in kcal/mol) for CO_2 insertion into 3 with different DFT functionals. Barriers are computed relative to 3 and free CO_2.

TS (see Figure S35)	PBE-D3BJ	B3LYP-D3BJ
inner sphere TS	7.7	10.4
outer sphere TS	22.7	24.3

References

(1) Torker, S.; Müller, A.; Sigrist, R.; Chen, P. Tuning the Steric Properties of a Metathesis Catalyst for Copolymerization of Norbornene and Cyclooctene toward Complete Alternation. *Organometallics* **2010**, *29* (12), 2735–2751.

(2) Kohler, L.; Hayes, D.; Hong, J.; Carter, T. J.; Shelby, M. L.; Fransted, K. A.; Chen, L. X.; Mulfort, K. L. Synthesis, Structure, Ultrafast Kinetics, and Light-Induced Dynamics of CuHETPHEN Chromophores. *Dalt. Trans.* **2016**, *45* (24), 9871–9883.

(3) Saito, T.; Uchida, Y.; Misono, A.; Yamamoto, A.; Morifuji, K.; Ikeda, S. Diethyldipyridylnickel. Preparation, Characterization, and Reactions. *J. Am. Chem. Soc.* **1966**, *88* (22), 5198–5201.

(4) Juliá-Hernández, F.; Moragas, T.; Cornella, J.; Martin, R. Remote Carboxylation of Halogenated Aliphatic Hydrocarbons with Carbon Dioxide. *Nature* **2017**, *545* (7652), 84–88. https://doi.org/10.1038/nature22316.

(5) Evans, D. F. 400. The Determination of the Paramagnetic Susceptibility of Substances in Solution by Nuclear Magnetic Resonance. *J. Chem. Soc.* **1959**, 2003–2005.

(6) Sur, S. K. Measurement of Magnetic Susceptibility and Magnetic Moment of Paramagnetic Molecules in Solution by High-Field Fourier Trasform NMR Spectroscopy. *J. Magn. Reson.* **1989**, *82*, 169–173.

(7) Meng, Q. Y.; Wang, S.; Huff, G. S.; Konig, B. Ligand-Controlled Regioselective Hydrocarboxylation of Styrenes with CO_2 by Combining Visible Light and Nickel Catalysis. *J. Am. Chem. Soc.* **2018**, *140* (9), 3198–3201.

(8) Hatnean, J. A.; Beck, R.; Borrelli, J. D.; Johnson, S. A. Carbon-Hydrogen Bond Oxidative Addition of Partially Fluorinated Aromatics to a $Ni(P^iPr_3)_2$ Synthon: The Influence of Steric Bulk on the Thermodynamics and Kinetics of C–H Bond Activation. *Organometallics* **2010**, *29* (22), 6077–6091.

(9) Johnson, S. A.; Huff, C. W.; Mustafa, F.; Saliba, M. Unexpected Intermediates and Products in the C−F Bond Activation of Tetrafluorobenzenes with a Bis(Triethylphosphine)Nickel Synthon: Direct Evidence of a Rapid and Reversible C−H Bond Activation by Ni(0). *J. Am. Chem. Soc.* **2008**, *130* (51), 17278–17280.

https://doi.org/10.1021/ja8081395.
(10) Li, T.; García, J. J.; Brennessel, W. W.; Jones, W. D. C–CN Bond Activation of Aromatic Nitriles and Fluxionality of the η^2-Arene Intermediates: Experimental and Theoretical Investigations. *Organometallics* **2010**, *29* (11), 2430–2445.
(11) Bach, I.; Pörschke, K.-R.; Goddard, R.; Kopiske, C.; Krüger, C.; Rufińska, A.; Seevogel, K. Synthesis, Structure, and Properties of $\{(^tBu_2PC_2H_4P^tBu_2)Ni\}_2(\mu\text{-}\eta^2\text{:}\eta^2\text{-}C_6H_6)$ and $(^tBu_2PC_2H_4P^tBu_2)Ni(\eta^2\text{-}C_6F_6)$. *Organometallics* **1996**, *15* (23), 4959–4966.
(12) Johnson, S. A.; Taylor, E. T.; Cruise, S. J. A Combined Experimental and Computational Study of Unexpected C–F Bond Activation Intermediates and Selectivity in the Reaction of Pentafluorobenzene with a $(PEt_3)_2Ni$ Synthon. *Organometallics* **2009**, *28* (13), 3842–3855.
(13) Gaussian 16, Revision B.01, Frisch, M. J.; Trucks, G. W.; Schlegel, H. B.; Scuseria, G. E.; Robb, M. A.; Cheeseman, J. R.; Scalmani, G.; Barone, V.; Petersson, G. A.; Nakatsuji, H.; Li, X.; Caricato, M.; Marenich, A. V.; Bloino, J.; Janesko, B. G.; Gomperts, R.; Mennucci, B.; Hratchian, H. P.; Ortiz, J. V.; Izmaylov, A. F.; Sonnenberg, J. L.; Williams-Young, D.; Ding, F.; Lipparini, F.; Egidi, F.; Goings, J.; Peng, B.; Petrone, A.; Henderson, T.; Ranasinghe, D.; Zakrzewski, V. G.; Gao, J.; Rega, N.; Zheng, G.; Liang, W.; Hada, M.; Ehara, M.; Toyota, K.; Fukuda, R.; Hasegawa, J.; Ishida, M.; Nakajima, T.; Honda, Y.; Kitao, O.; Nakai, H.; Vreven, T.; Throssell, K.; Montgomery, J. A., Jr.; Peralta, J. E.; Ogliaro, F.; Bearpark, M. J.; Heyd, J. J.; Brothers, E. N.; Kudin, K. N.; Staroverov, V. N.; Keith, T. A.; Kobayashi, R.; Normand, J.; Raghavachari, K.; Rendell, A. P.; Burant, J. C.; Iyengar, S. S.; Tomasi, J.; Cossi, M.; Millam, J. M.; Klene, M.; Adamo, C.; Cammi, R.; Ochterski, J. W.; Martin, R. L.; Morokuma, K.; Farkas, O.; Foresman, J. B.; Fox, D. J. Gaussian, Inc., Wallingford CT, **2016**.
(14) Perdew, J. P.; Burke, K.; Ernzerhof, M. Generalized Gradient Approximation Made Simple. *Phys. Rev. Lett.* **1996**, *77* (18), 3865.
(15) Perdew, J. P.; Burke, K.; Ernzerhof, M. Generalized Gradient Approximation Made Simple [Phys. Rev. Lett. 77, 3865 (1996)]. *Phys. Rev. Lett.* **1997**, *78* (7), 1396.
(16) Becke, A. D. Density-Functional Thermochemistry. III. The Role of Exact Exchange. *J. Chem. Phys.* **1993**, *98* (5), 645–648.
(17) Grimme, S.; Ehrlich, S.; Goerigk, L. Effect of the Damping Function in Dispersion Corrected Density Functional Theory. *J. Comput. Chem.* **2011**, *32* (7), 1456–1465.
(18) Tomasi, J.; Mennucci, B.; Cammi, R. Quantum Mechanical Continuum Solvation Models. *Chem. Rev.* **2005**, *105* (8), 2999–3094.
(19) Tomasi, J.; Mennucci, B.; Cances, E. The IEF Version of the PCM Solvation Method: An Overview of a New Method Addressed to Study Molecular Solutes at the QM Ab Initio Level. *J. Mol. Struct. THEOCHEM* **1999**, *464* (1–3), 211–226.
(20) Cances, E.; Mennucci, B.; Tomasi, J. A New Integral Equation Formalism for the Polarizable Continuum Model: Theoretical Background and Applications to Isotropic and Anisotropic Dielectrics. *J. Chem. Phys.* **1997**, *107* (8), 3032–3041.
(21) Computational Chemistry Comparison and Benchmark DataBase, National Institute of Standards and Technology (NIST) cccbdb.nist.gov/vibscalejust.asp (accessed Jan 10, 2019).